Atmospheric Environment 174 (2018) 1–14

Contents lists available at ScienceDirect

Atmospheric Environment

journal homepage: www.elsevier.com/locate/atmosenv

Coordinated profiling of stratospheric intrusions and transported pollution by the Tropospheric Ozone Lidar Network (TOLNet) and NASA Alpha Jet experiment (AJAX): Observations and comparison to HYSPLIT, RAQMS, and FLEXPART

A.O. Langford[a,*], R.J. Alvarez II[a], J. Brioude[a,b,c], S. Evan[a,b,c], L.T. Iraci[d], G. Kirgis[a,b,e], S. Kuang[f], T. Leblanc[e], M.J. Newchurch[g], R.B. Pierce[h], C.J. Senff[a,b], E.L. Yates[d,i]

[a] NOAA Earth System Research Laboratory, Chemical Sciences Division, Boulder, CO 80305, USA
[b] Cooperative Institute for Research in Environmental Sciences, University of Colorado, Boulder, CO 80309, USA
[c] Laboratoire de l'Atmosphere et des Cyclones (LACy), UMR 8105, CNRS, Université de La Réunion, Météo-France, Saint-Denis, La Reunion, France
[d] Atmospheric Science Branch, NASA Ames Research Center, Moffett Field, CA 94035, USA
[e] Jet Propulsion Laboratory, California Institute of Technology, Wrightwood, CA 92397, USA
[f] Earth System Science Center, University of Alabama in Huntsville, Huntsville, AL 35805, USA
[g] Atmospheric Science Department, University of Alabama in Huntsville, Huntsville, AL 35805, USA
[h] NOAA/NESDIS Center for Satellite Applications and Research, Cooperative Institute for Meteorological Satellite Studies, Madison, WI 53706, USA
[i] Bay Area Environmental Research Institute, Petaluma, CA 94952, USA

ARTICLE INFO

Keywords:
Background ozone
Stratospheric intrusion
Long-range transport
NAAQS
Lidar
Exceptional events

ABSTRACT

Ground-based lidars and ozonesondes belonging to the NASA-supported Tropospheric Ozone Lidar Network (TOLNet) are used in conjunction with the NASA Alpha Jet Atmospheric eXperiment (AJAX) to investigate the transport of stratospheric ozone and entrained pollution into the lower troposphere above the United States on May 24–25, 2013. TOLNet and AJAX measurements made in California, Nevada, and Alabama are compared to tropospheric ozone retrievals from the Atmospheric Infrared Sounder (AIRS), to back trajectories from the NOAA Air Resources Laboratory (ARL) Hybrid Single Particle Lagrangian Integrated Trajectory (HYSPLIT) model, and to analyses from the NOAA/NESDIS Real-time Air Quality Modeling System (RAQMS) and FLEXPART particle dispersion model. The measurements and model analyses show much deeper descent of ozone-rich upper tropospheric/lower stratospheric air above the Desert Southwest than above the Southeast, and comparisons to surface measurements from regulatory monitors reporting to the U.S. EPA Air Quality System (AQS) suggest that there was a much greater surface impact in the Southwest including exceedances of the 2008 National Ambient Air Quality Standard (NAAQS) of 0.075 ppm in both Southern California and Nevada. Our analysis demonstrates the potential benefits to be gained by supplementing the existing surface ozone network with coordinated upper air observations by TOLNet.

1. Introduction

It is well established that even moderate concentrations of ozone (O_3) can harm human health (EPA, 2013) and impair plant growth and productivity (EPA, 2013; Lefohn et al., 1988). Ozone was accordingly designated a criteria air pollutant by the 1970 U.S. Clean Air Act (CAA), and the U.S. Environmental Protection Agency (EPA) established National Ambient Air Quality Standards (NAAQS) to protect human health and welfare from its adverse effects. The CAA requires that the NAAQS for ozone and other criteria pollutants be periodically reviewed and adjusted, if necessary, to provide an adequate margin of safety for the public. The most recent such review led to the lowering of the ozone NAAQS from the value of 0.075 parts-per-million (ppm) for the 3-yr average of the 4th highest maximum daily 8-h average (MDA8) concentration set in 2008 to a value of 0.070 ppm in October of 2015 (U.S. Environmental Protection Agency, 2015).

Ozone is a secondary pollutant formed through photochemical reactions between nitrogen oxides (NOx) and volatile organic compounds (VOCs), and efforts to control ambient concentrations have sought to regulate anthropogenic emissions of these precursors. Ozone also has

* Corresponding author.
E-mail address: andrew.o.langford@noaa.gov (A.O. Langford).

https://doi.org/10.1016/j.atmosenv.2017.11.031
Received 18 September 2017; Received in revised form 14 November 2017; Accepted 18 November 2017
Available online 21 November 2017

significant background concentrations, however, that lie outside local control and complicate regulatory efforts. Background ozone is derived from NOx and VOCs emitted from distant anthropogenic sources, as well as from natural sources, such as soils, vegetation, lightning, wildfires, and from naturally formed ozone transported downward from the lower stratosphere (EPA, 2014).

Most stratosphere-to-troposphere transport (STT) at midlatitudes occurs through the formation of tropopause folds (Danielsen, 1968), tongues of upper tropospheric and lower stratospheric (UT/LS) air (Wernli and Davies, 1997) extruded downward into the free troposphere beneath the jet stream circulating around extratropical cyclones. Tropopause folds can occur year-round, but are most frequent during fall, winter, and spring in the Northern Hemisphere (Elbern et al., 1998) and probably form during the life cycle of most midlatitude cyclones (Johnson and Viezee, 1981). The majority are dissipated in the middle and upper troposphere by turbulence (Shapiro, 1980), convection (Cho et al., 1999; Langford and Reid, 1998), or breaking gravity waves (Langford et al., 1996), or are irreversibly stretched into streamer-like structures (Appenzeller and Davies, 1992) that slowly become part of the tropospheric background (Bithell et al., 2000). Those that reach the lower troposphere are usually highly diluted (Trickl et al., 2014), but on rare occasions, deep tropopause folds can cause large spikes in surface ozone (Attmannspacher and Hartmannsgruber, 1973; Davies and Schuepbach, 1994; Haagenson et al., 1981; Lamb, 1977; Stohl et al., 2000; Viezee et al., 1983). A growing number of studies (Hess et al., 2015; James et al., 2003; Skerlak et al., 2014; Wernli and Bourqui, 2002) have shown that the West Coast of North America is one of the preferred locations for deep tropopause folds (Bourqui and Trepanier, 2010), which can also entrain wildfire plumes (Brioude et al., 2007) or anthropogenic pollution transported across the Pacific Ocean from Asia during their descent (Cooper et al., 2004; Lin et al., 2012) and carry these contaminants toward the surface.

Deep STT episodes have been implicated in exceedances of the ozone NAAQS in the western U.S. (Kaldunski et al., 2017; Langford et al., 2009, 2015), and Section 319b of the U.S. Clean Air Act establishes a mechanism known as the Exceptional Events Rule (EER) to exclude those exceedances caused by stratospheric intrusions, wildfires (Jaffe et al., 2013), or other natural events from regulatory consideration (U.S. Environmental Protection Agency, 2007; 2016). Likewise, Section 179B provides a mechanism to exclude exceedances caused by intercontinental transport of pollution. It has proven challenging for state, tribal, and local regulatory agencies to implement these rules, however, in large part because of the difficulty in quantifying or even identifying the impact of STT and long-range transport (LRT) on surface ozone using only regulatory surface monitors, and only one ozone exceptional events report has been accepted by the EPA to date (Kaldunski et al., 2017; State of Wyoming, 2013). One reason for this difficulty is the sparsity of ground-based ozone monitors in the western U.S. (Gustin et al., 2015) where the impact of STT on surface ozone appears to be greatest (Lefohn et al., 2014, 2011, 2012; Lin et al., 2012). Another is the fact that stratospheric intrusions and associated pollution transport events do not always produce easily flagged spikes in surface O_3, but instead may cause the concentrations to increase slowly as the descending air is entrained into the mixed layer (Kunz and Speth, 1997; Langford et al., 2017; Viezee et al., 1983). Even these “unexceptional” events can cause exceedances of the 2015 NAAQS if they add 10 to 20 parts-per-billion by volume (ppbv) to the typical O_3 concentrations of 50–60 ppbv found in the southwestern U.S. during late spring (Fiore et al., 2014).

The most serious obstacle preventing state and local regulatory agencies from distinguishing the influence of STT and long-range transport on surface ozone is a lack of knowledge about the ozone concentrations above the surface (Cooper et al., 2015). Ozonesondes are routinely launched only about once per week from a small number of locations in the U.S. (Newchurch et al., 2003) and ozone retrievals using current space-based sensors have limited sensitivity and vertical resolution in the lower troposphere (Duncan et al., 2014; Zoogman et al., 2011). These observational deficiencies also make it difficult to evaluate the performance of satellite retrievals and the regional and global chemical transport models (Fiore et al., 2014; Lin et al., 2012; Zhang et al., 2011, 2014) that could potentially be used to quantify the impacts of STT on surface ozone for EER purposes.

The dearth of vertical ozone profiling in North America motivated the creation of the NASA-sponsored Tropospheric Ozone Lidar Network (TOLNet) to coordinate the activities of existing ground-based tropospheric ozone lidars in the U.S. and Canada. TOLNet includes fixed and transportable lidar systems that operate both routinely and on a campaign basis. Much of the data is posted on the TOLNet website (http://www-air.larc.nasa.gov/missions/TOLNet/index.html) and other measurements can be made available to state, tribal, and local regulatory agencies on request. TOLNet measurements can potentially be used to supplement routine surface monitoring, to investigate the synoptic-scale behavior of tropospheric ozone, and to help assess the impact of stratospheric intrusions and transported ozone on surface air quality. TOLNet measurements will also be used to help validate the high temporal and spatial resolution data obtained from the upcoming GEO-CAPE (Fishman et al., 2012) and TEMPO (Zoogman et al., 2014) satellite missions.

In this paper, we use TOLNet measurements made in California, Nevada, and Alabama to characterize the descent of two stratospheric intrusions that developed above the contiguous U.S. on May 24–25, 2013. The lidar measurements in California and Nevada were coordinated with an AJAX research flight, and the Nevada and Alabama measurements were part of larger efforts in support of the Las Vegas Ozone Study (LVOS) (Langford et al., 2015, 2017) and Southeast Nexus (SENEX) (Kuang et al., 2017; Warneke et al., 2016) field campaigns. Both intrusions were forecast by the NOAA National Environmental Satellite, Data, and Information System (NESDIS) Real-time Air Quality Modeling System (RAQMS) assimilation/forecast model (Pierce et al., 2003, 2007) and FLEXPART particle dispersion models (Brioude et al., 2013; Stohl et al., 2005) used in support of these campaigns. We compare the lidar and aircraft measurements to TOLNet ozonesonde profiles and to retrievals from the Atmospheric Infrared Sounder (AIRS) (Martin, 2008; Zoogman et al., 2011) aboard the NASA *Aqua* satellite, as well as back trajectories from the NOAA Air Resources Laboratory (ARL) Hybrid Single Particle Lagrangian Integrated Trajectory (HYSPLIT) model (Rolph et al., 2017; Stein et al., 2015) and the RAQMS and FLEXPART analyses. Finally, we use surface measurements from regulatory monitors reporting to the U.S. EPA Air Quality System (AQS) to show how the stratospheric intrusions sampled by the coordinated TOLNet lidar and AJAX aircraft observations impacted surface air quality on May 23–25, 2013.

2. Tropospheric Ozone Lidar Network (TOLNet)

The Tropospheric Ozone Lidar Network or TOLNet was organized in 2010 under the auspices of the NASA Earth Sciences Division. The network loosely coordinates the activities of existing ground-based tropospheric ozone lidar systems in the U.S. and Canada and provides recommendations for the development of future systems. Three of the six lidar systems currently belonging to the network are operated by NASA through the Jet Propulsion Laboratory (JPL) Table Mountain Facility (TMF) in California (McDermid et al., 2002), the Langley Research Center (LaRC) in Virginia (Sullivan et al., 2015a), and the Goddard Space Flight Center (GSFC) in Maryland (Sullivan et al., 2015b). The remaining three are operated by the NOAA Earth System Research Laboratory (ESRL) (Alvarez et al., 2011), the University of Alabama at Huntsville (UAH) (Kuang et al., 2013), and Environment and Climate Change Canada (ECCC) (Strawbridge et al., 2017).

All of the TOLNet lidars use the differential absorption lidar (DIAL) technique (Proffitt and Langford, 1997) to measure ozone, but with hardware configurations and operating characteristics determined by

the primary research missions of the individual research groups. Several of the TOLNet groups also launch ozonesondes with electrochemical cell (ECC) sensors (Johnson et al., 2002) to support their lidar operations. Five of the TOLNet lidar systems were designed specifically for (zenith) vertical profiling of the free troposphere from fixed (TMF and UAH) or mobile (LaRC, GSFC, and ECCC) ground-based platforms. The sixth, the NOAA ESRL TOPAZ (Tunable Optical Profiler for Aerosols and oZone) scanning lidar, was originally designed for airborne nadir profiling of the boundary layer (Alvarez et al., 2011; Langford et al., 2011), but subsequently reconfigured for mobile ground-based operation. Only the TMF, UAH, and ESRL systems were fully operational as of May 24, 2013.

TMF (34.38°N, 117.68°W, 2 286 m asl) is located just north of the Los Angeles Basin in the San Gabriel Mountains. This NASA JPL facility also has dedicated stratospheric ozone (McDermid et al., 1990) and water vapor Raman (Leblanc et al., 2012) lidars that contribute to the International Network for the Detection of Atmospheric Composition Change (NDACC) (Kirgis et al., 2013). UAH (34.73°N, 86.65°W, 206 m asl) (Kuang et al., 2011, 2013) is located in northern Alabama near the Tennessee border about 2 800 km due east of TMF. Both of these lidars use relatively high power, low repetition rate, fixed wavelength laser sources with multiple receiver systems optimized to profile ozone from about 800 to 300 m above the surface, respectively, into the lower stratosphere. The TMF and UAH measurements on May 24–25 were made with integration times of 5 and 15–20 min, respectively, and the profiles analyzed with vertical resolutions ranging from 400 to 1 200 m in the troposphere.

The truck-mounted NOAA ESRL TOPAZ lidar was deployed from its home base in Boulder, CO to a high-elevation site at Angel Peak (AP), NV (AP, 36.32 °N, 115.57 °W, 2 682 m asl) during May and June of 2013 for the Las Vegas Ozone Study (LVOS) (Langford et al., 2015). This vertically pointing system uses a large scanning mirror to make slant path measurements at different elevation angles in order to profile the boundary layer and lower troposphere. During LVOS, TOPAZ measured 75-s slant profiles at elevations of 2, 6, 20, and 90 above the horizon in a cycle that repeated every 5 min. The slant path profiles were smoothed with a constant 450-m running average and then projected along the zenith to create overlapping vertical profiles. This technique allowed TOPAZ to measure O_3 within 20 m of the surface with an effective vertical resolution ranging from ~10 m below 50 m above ground level, (agl), ~30 m between 50 and 150 m agl, ~100 m between 150 and 500 m agl, and 315 m above 500 m agl. Because it was originally developed for airborne operations where eye safety is of paramount concern, the TOPAZ lidar operates at a much higher repetition rate with lower peak energies than the TMF and UAH lidars. These low energies, coupled with the legacy data acquisition system from the aircraft, limited the maximum vertical range to about 2.5 or 3 km during LVOS.

3. Alpha Jet Atmospheric experiment (AJAX)

The NASA Ames Alpha Jet eXperiment (AJAX) (Hamill et al., 2016) samples O_3 and other tropospheric constituents above California and Nevada using a two-person light subsonic attack jet and advanced trainer based at Moffett Field, CA (MF, 37.415° N, −122.050° E). The primary aim of the AJAX project is the characterization of greenhouse gases above California and Nevada, but some AJAX flights have focused on the distribution of O_3 (Ryoo et al., 2017; Yates et al., 2013) including the influence of long-range transport (Yates et al., 2015) and stratospheric intrusions (Yates et al., 2011). The Alpha Jet carries an external wing pod with a modified commercial UV absorption monitor (2B Technologies Inc., model 205) to measure O_3 (Yates et al., 2011, 2015) and a (Picarro model 2 301-m) cavity ringdown analyzer to measure CO_2, CH_4, and H_2O (Tanaka et al., 2016). The 2B O_3 data, taken every 2 s, are averaged over 10 s to increase the signal-to-noise ratio, giving an overall ozone uncertainty of 3 ppbv at 10-s resolution. The overall uncertainties for the CO_2 and CH_4 measurements are typically less than 0.16 ppmv and 2.2 ppbv, respectively, when the 3-Hz data were binned to 3 s (Tanaka et al., 2016). The aircraft has GPS and inertial navigation systems to provide altitude, temperature and position information, and has added capabilities for three-dimensional wind and formaldehyde (CH_2O) measurements since the May 2013 flights. The Alpha Jet flew from MF to TMF and back on the afternoon of May 24, 2013, and conducted a spiral descent over TMF.

4. Atmospheric Infrared Sounder (AIRS)

The Atmospheric Infrared Sounder (AIRS) (Martin, 2008; Zoogman et al., 2011) aboard the NASA EOS/*Aqua* sun synchronous polar orbiting satellite measures upwelling thermal infrared radiation (TIR, 650 to 2 700 cm^{-1}) that can be used to retrieve near real time tropospheric concentrations of O_3, CO, CH_4, and H_2O at standard pressure levels. These wavelengths can be used to probe deep into the troposphere both day and night, unlike nadir ultraviolet (UV) reflectance measurements that are limited to daytime operation and higher altitudes. *Aqua* orbits the Earth 14.5 times per day and covers an orbital distance of ~1 500 km during each 6-min file period. The nadir-viewing AIRS sounder has a 15-km field of view and uses the whisk broom scanning method to cover a swath ~1 500 km wide perpendicular to the circumpolar orbital motion. Several studies have shown the version 4 O_3 AIRS ozone retrievals to be biased high in the upper troposphere compared to ozonesondes (Bian et al., 2007; Divakarla et al., 2008; Monahan et al., 2007), but this bias has been reduced by using tropopause-based reference climatologies with the version 5 O_3 AIRS data products (Pittman et al., 2009; Wei et al., 2010). Here we use the May 24, 2013 measurements from the more recent version 6, Level 2 cloud-cleared retrievals for O_3, CO, CH_4 and H_2O (https://disc.gsfc.nasa.gov/datareleases/aqua-airs-version-6).

5. RAQMS and FLEXPART models

The NOAA/NESDIS RAQMS (Realtime Air Quality Modeling System) model is a unified (stratosphere-troposphere) online global chemical and aerosol assimilation/forecasting system developed to support airborne field missions (Pierce et al., 2003, 2007). The meteorological forecasts are conducted using the University of Wisconsin Hybrid Model (Schaack et al., 2004), and the chemical forecasts are initialized daily at 12 UT with real-time assimilation of Ozone Monitoring Instrument (OMI) cloud-cleared total column ozone and Microwave Limb Sounder (MLS) ozone profiles from the NASA *Aura* satellite, and MODIS aerosol optical depth from the NASA *Terra* and *Aqua* satellites. RAQMS has been run routinely in a forecast mode since 2010 with 2° × 2° resolution analyses and forecasts prior to 2012, and 1° × 1° analyses since 2012. The model predicts the instantaneous global O_3 CO, SO_4, and black organic carbon distributions at 6-h intervals for the next 4 days. The real-time analyses are used for most mission studies, including LVOS, and the routine RAQMS plots archived online (http://raqms-ops.ssec.wisc.edu).

FLEXPART (Stohl et al., 2005) is a Lagrangian particle dispersion model that calculates the evolving distribution of a multitude of "particles" transported forward in time from a specified source region, or backward in time from a specific receptor location. The passive particles are transported by the resolved winds and by parameterized sub grid motions including turbulence and convection. FLEXPART implements the convection parameterization scheme of Emanuel and Zivkovic-Rothman (1999) at 15-min model time steps and parameterizes turbulence in the boundary layer using the Hanna turbulence scheme (Hanna, 1982). The *Emanuel and Zivkovic-Rothman* scheme is intended to describe all types of convection, and includes entrainment and mixing, cloud microphysical processes, and large-scale control of ensemble convective activity including the interaction between convective downdrafts and surface fluxes.

FLEXPART was run in the source (forward) mode during LVOS and SENEX to generate stratospheric ozone, Asian CO, and biomass burning CO forecast products for LVOS and the overlapping (May 29 - July 10) SENEX (Southeast Nexus) campaign (Warneke et al., 2016). Tracer distributions were calculated hourly for an output domain extending from −140 to −90°E and from 25 to 70°N. Horizontal distributions were plotted and archived online for both the boundary layer (below 1.5 km asl) and for the lower free troposphere (3–6 km asl). The stratospheric O_3 tracer used here was represented by particles released into the stratosphere (> 2 potential vorticity units or PVU) with the O_3 mixing ratios calculated using a linear relationship between O_3 and potential vorticity (60 ppbv/PVU) at the particle origin. The O_3 mixing ratio is conserved and the particle distribution recalculated for up to 20 days with no chemistry.

Uncertainty in the driving meteorology is one of the major sources of inaccuracy in the FLEXPART output. During LVOS and SENEX, the FLEXPART forecasts were run using the National Centers for Environmental Prediction (NCEP) Global Forecast System (GFS) forecasts (analyses at 00, 06, 12, and 18 UT; 3-h forecasts at 03, 09, 15, and 21 UT) and run at a spatial resolution of 0.5° × 0.5° with 26 vertical levels. These forecasts were continuously updated as newer GFS input data became available. For the comparisons shown below, the FLEXPART model was re-run using meteorology from the European Center for Medium-Range Weather Forecasts (ECMWF) with a spatial resolution of 0.25° × 0.25° and 90 vertical levels.

6. Case study: May 24–25, 2013

6.1. Meteorological context

A series of closely spaced midlatitude cyclones brought severe weather to much of the U.S. during the second half of May 2013, including multiple tornado outbreaks, hailstorms, and record precipitation events across the eastern U.S. and Southern Great Plains (Gravelle et al., 2016; NOAA, 2014). Two of these low-pressure systems spun up into closed lows as they moved ashore into the Pacific Northwest (PNW), and spawned large tropopause folds above the West Coast on May 20–21 and May 24–25 (Langford et al., 2017) similar to those observed during the CalNex and IONS-2010 campaigns in May of 2010 (Cooper et al., 2011; Langford et al., 2012; Lin et al., 2012). The leading cyclone weakened as it crossed the Rocky Mountains, but re-intensified into an elongated trough east of the Mississippi River where it developed a second tropopause fold on May 24–25. These two deep low-pressure systems, separated by a strong blocking high, are shown in Fig. 1a, which displays the National Centers for Environmental Prediction/North American Regional Reanalysis (NCEP/NARR) 350 hPa (~8 km above mean sea level, asl) geopotential heights for 12 UT on May 24, 2013 obtained from the NOAA ESRL Physical Sciences Division (Mesinger and Coauthors, 2006). The locations of the active TOLNet lidars and AJAX flight track on May 24 are also shown.

Tropopause folds usually develop during cyclogenesis, the spin up or re-intensification of the cyclonic circulation (Danielsen, 1968; Reed and Danielsen, 1959). These isentropically sloping tongues of UT/LS air are created by ageostrophic circulations at the entrance region of jet streaks (Hoskins, 1982; Keyser and Shapiro, 1986), i.e. localized wind maxima produced when the vertically meandering jet intersects a constant pressure surface (Bluestein, 1993). The 350 hPa NCEP/NARR winds in Fig. 1b show that there were moderate-to-strong jet streaks (> 40 m/s) on the western flank of the leading cyclone above Indiana, Ohio, and Kentucky, and on the southeastern flank of the trailing cyclone above Montana and Wyoming at 12 UT on May 24, 2013. The corresponding GOES water vapor images (Fig. 2a) show pronounced dry bands (i.e. regions of warmer temperatures corresponding to deeper tropospheric penetration when there is little attenuation by water vapor) on the equatorward side of both jet streaks that are consistent with descent of UT/LS air into the middle troposphere (Appenzeller and Davies, 1992; Manney and Stanford, 1987). The western-most of these dry bands drifted eastward over the TOLNet lidar sites in California and Nevada over the next several hours (Fig. 2b) before becoming obscured by filaments of high cirrus created by dispersing aircraft contrails above central California (Fig. 2c). The eastern-most dry band moved southward across the UAH lidar in Alabama over the same period.

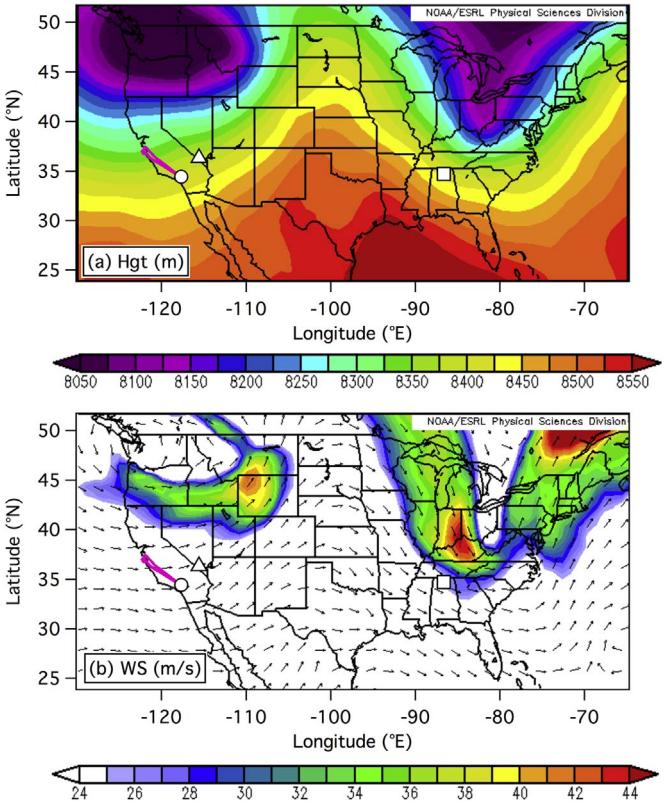

Fig. 1. NCEP/NARR (1° x 1°) 350 hPa (a) geopotential heights (m), and (b) vector winds (m s-1) for 12 UT May 24, 2013. The filled white symbols in this and subsequent figures mark the locations of the TMF (circle), AP (triangle), and UAH (square) lidars. The magenta lines mark the flight path of the NASA AJAX mission from Moffett Field to and from TMF. NARR images provided by the NOAA/ESRL Physical Science Division, Boulder Colorado from their Web site at http://www.AP.noaa.gov/psd/.

Fig. 3 shows the 1° × 1° RAQMS 12 UT May 24, 2013 O_3 distributions on the (a) 500, (b) 700, and (c) 850 hPa pressure surfaces, which roughly correspond to altitudes of 5.8, 3.1, and 1.5 km asl. Fig. 3a shows areas of high (100–120 ppbv) O_3 consistent with descending lower stratospheric air on the 500 hPa surface beneath each of the jet streaks in Fig. 1b, with filaments of moderately high (> 80 ppbv) O_3 stretching anticyclonically from each hotspot (cf. Fig. 1b). The western-most filament sweeps through Nevada and California above TMF and AP and across the AJAX flight track. The eastern-most filament covers much of the eastern U.S. and passes above UAH. The filaments are also present on the 700 hPa surface (Fig. 3b) with moderately high O_3 concentrations above or near all three of the TOLNet stations. The O_3 enhancement within both filaments is about 20 ppbv on both the 500 and 700 hPa surfaces. The total O_3 on the 850 hPa surface (~1.5 km asl) is much smaller, with peak concentrations of ~65 ppbv off the coast of Baja California.

The RAQMS analyses do not isolate the contributions of long-range transport and stratospheric intrusions from the O_3 originating from local and regional photochemical production. The stratospheric contribution is isolated in Fig. 4, which shows the instantaneous 12UT May 24, 2013 FLEXPART STT tracer distributions on the same pressure surfaces calculated using the European Center for Medium-Range Weather Forecasts (ECMWF) winds at 0.25° × 0.25° resolution. The FLEXPART STT tracer distribution on the 500 hPa surface (Fig. 4a) is

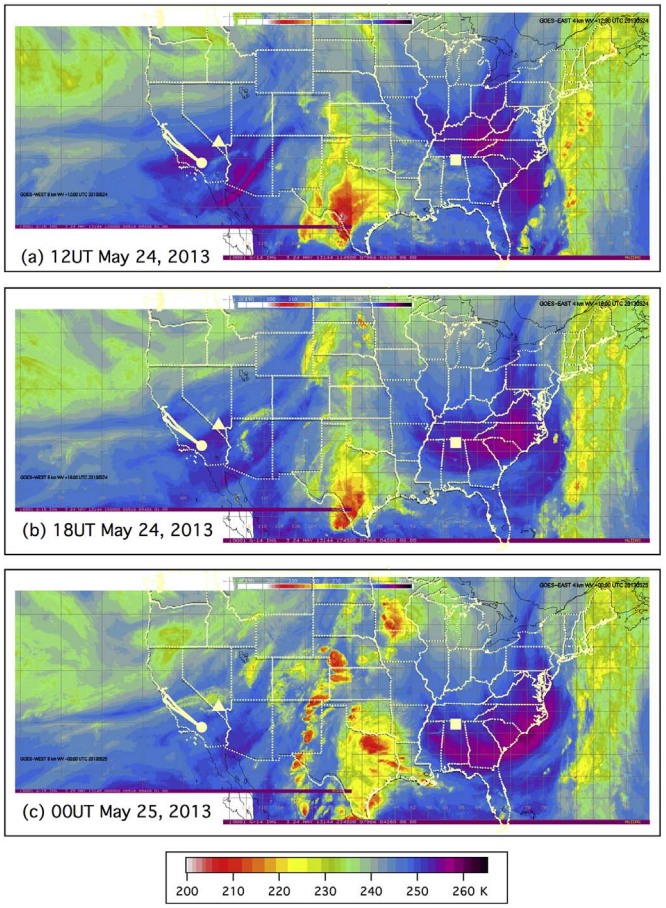

Fig. 2. GOES-WEST (left) and GOES-EAST (right) 4-km colorized water vapor images for (a) 12 UT May 24, 2013, (b) 18 UT May 24, 2013, and (c) 00 UT May 25, 2013. The locations of the lidars and AJAX flight path are shown in white. Images provided by Owen Cooper.

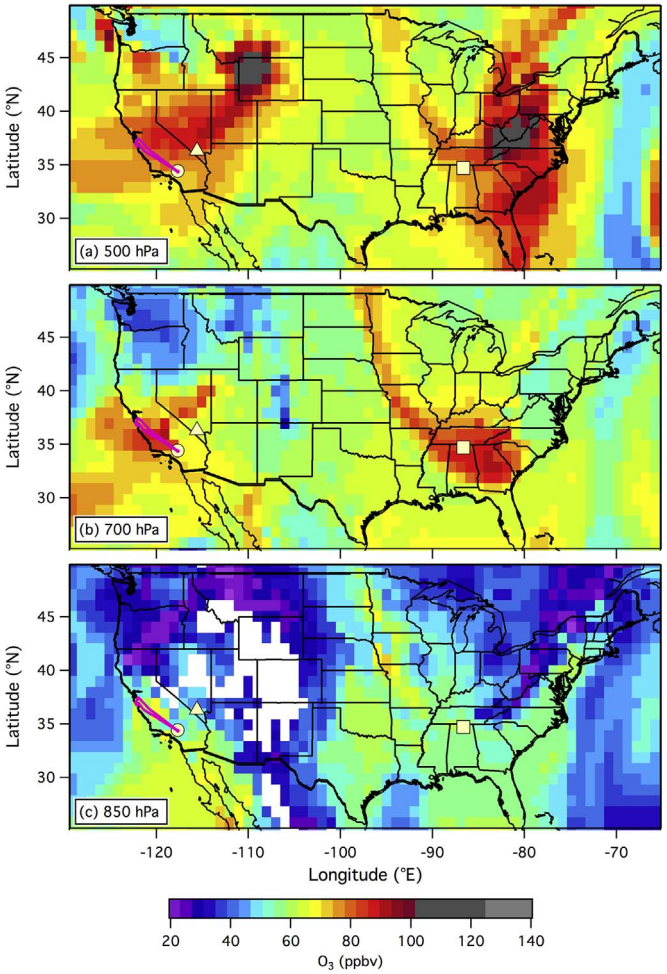

Fig. 3. RAQMS analyses of total O3 (1° × 1°) above the contiguous U.S. on the (a) 500, (b) 700, and (c) 850 hPa geopotential surfaces for 12 UT on May 24, 2013. The white areas around the Rocky Mountains in (c) correspond to elevations that lie above the 850 hPa surface.

qualitatively similar to the corresponding RAQMS distribution (cf. Fig. 3a), but has much higher peak concentrations beneath the two jet streaks: ~220 ppbv above northwestern Wyoming and ~110 ppbv above eastern Tennessee. The filaments appear finer and more detailed in the higher resolution FLEXPART analysis, with concentrations approaching 100 ppbv above northwestern Utah and central Nevada. The FLEXPART tracer distribution on the 700 hPa surface (Fig. 4b) is qualitatively similar to the RAQMS analyses above the western U.S., but again has much higher O_3 concentrations in the West (50–100 ppbv above Nevada). The peak FLEXPART STT magnitude of ~25 ppbv off the coast of Baja California on the 850 hPa surface (Fig. 4c) is in good agreement with RAQMS, however.

The 700 hPa FLEXPART STT tracer distributions above the eastern U.S. are smaller than the RAQMS enhancements with peak tracer concentrations of about 10 ppbv or less than half the peak RAQMS enhancements of 20–25 ppbv above Georgia (cf. Fig. 3b). The FLEXPART maximum is also shifted well to the south of the RAQMS maximum into the Gulf of Mexico. One possible explanation for these differences is that there was a large anthropogenic or biomass burning component in the RAQMS O_3 filament above the Southeast in Fig. 3b. However, this is not supported by the corresponding RAQMS CO analyses (not shown) that indicate CO to be depressed in this region.

6.2. Lidar measurements

Fig. 5 displays time-height curtain plots of the ozone profiles measured by the TMF, AP, and UAH tropospheric O_3 lidars in (a) California, (b) Nevada, and (c) Alabama, respectively, (cf. Fig. 1) over the 24-h period beginning at 16 UT on May 24, 2013, or 4 h after the model analyses in Figs. 1–4. Fig. 6 is an expanded view of these measurements showing the O_3 mixing ratios from the lowest 4 km above each lidar between 20 UT on May 24 and 04 UT on May 25. The colored horizontal bars represent the surface concentrations measured by ozone monitors at TMF, AP, and the Old Huntsville Airport, which is located ~6 km from the UAH lidar. The dotted black curves plot the local solar elevation angle. The horizontal dot, dash, long dash, and dot-dash black lines mark the 850, 700, 500, and 400 hPa pressure levels, respectively.

Figs. 5a and 6a also show the ozone mixing ratios measured by AJAX during its spiral descent over TMF, and by the ozonesonde launched from TMF shortly after AJAX departed. Figs. 5c and 6c likewise show the profile from an ozonesonde launched at UAH during a break in the lidar measurements. The open symbols in Fig. 6 mark the top of the mixed layer above each site as determined from either the local 2 130 UT ozonesonde (TMF, circle and UAH, square) or the 0 000 UT KVEF radiosonde (triangle) launched about 45 km southeast of Angel Peak at the Las Vegas McCarran International Airport. These afternoon mixed layer depths ranged from 1.6 km asl at UAH to 2.65 km asl at TMF and 3.9 km asl at AP. Note that the top of the mixed layer was only a few hundred meters above TMF.

All three of the curtain plots in Fig. 5 show multiple layers of high O_3 consistent with descent of UT/LS air above each of the lidars as suggested by the RAQMS and FLEXPART analyses. This supposition is also supported by Fig. 7, which plots 7-day Hybrid Single Particle Lagrangian Integrated Trajectory (HYSPLIT) back trajectories (0.5° Global

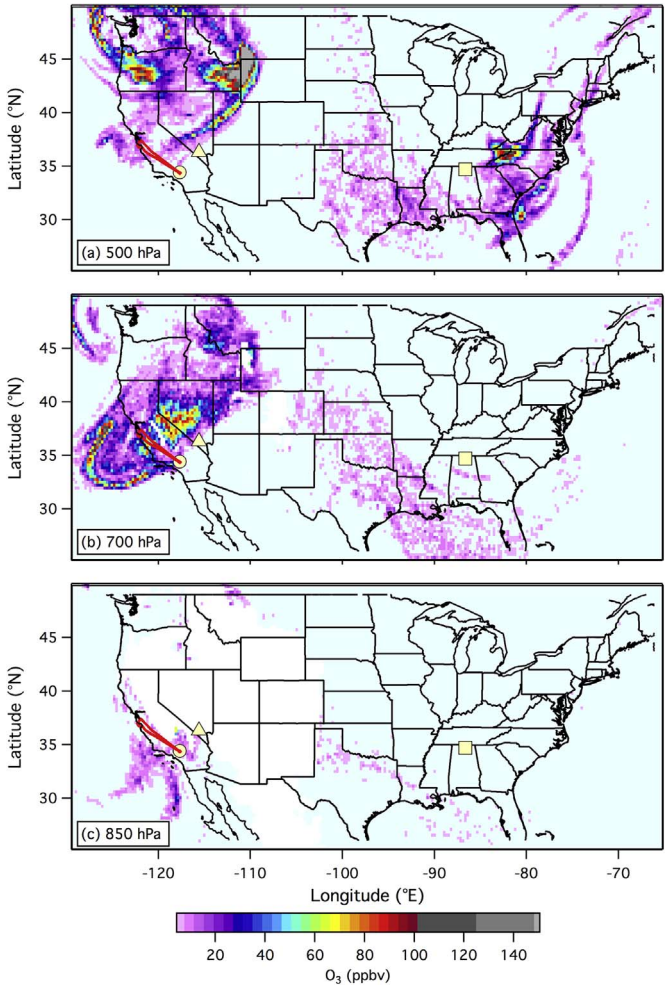

Fig. 4. FLEXPART stratospheric O3 tracer distributions calculated using the 0.25° × 0.25° ECMWF wind fields for 12 UT on May 24, 2013. (a) 500 hPa, (b) 700 hPa, and (c) 850 hPa. The white areas around the Rocky Mountains in (b) and (c) correspond to higher elevations that lie above the 700 and 850 hPa pressure surfaces.

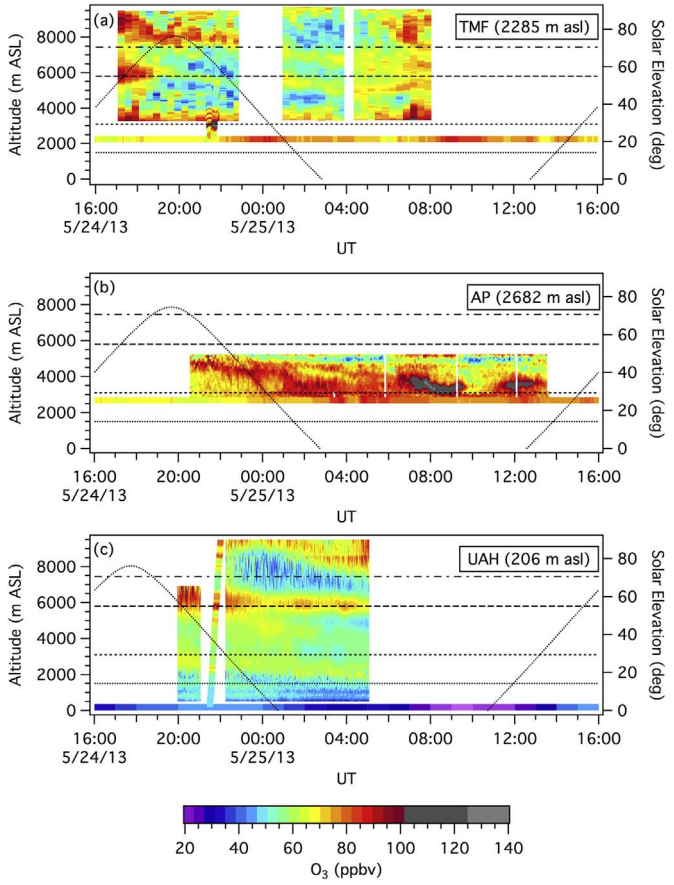

Fig. 5. Time-height curtain plots of the O3 mixing ratios measured by the (a) TMF, (b) AP, and (c) UAH lidars on May 24–25, 2013. The colored horizontal lines represent local surface measurements. The dot, dash, long dash, and dot-dash horizontal lines roughly correspond to the 850, 700, 500, and 350 hPa pressure altitudes. The dashed black curves show the local solar elevation angle. The nearly vertical stripes in (a) and (c) show the profiles from the TMF ozonesonde and Alpha Jet, and UAH ozonesonde, respectively. (For interpretation of the references to colour in this figure legend, the reader is referred to the web version of this article.)

Data Assimilation System, GDAS meteorology) originating from 700, 500, and 400 hPa above each of the 3 lidar sites. The 500 hPa back trajectories from TMF and AP, and the 700 hPa trajectory from UAH all show deep descent from above 16 km asl within the previous 5 days. The 400 hPa TMF, and the 700 and 400 hPa UAH back trajectories follow upper tropospheric paths from lower elevations in Asia. Only the 700 and 400 hPa trajectories from AP show recent North American surface influences.

The curtain plots in Figs. 5 and 6 show that the O_3-rich stratospheric air descended much deeper into the troposphere above the higher elevation western sites (TMF and AP) sites than above UAH in good agreement with the FLEXPART analyses. The lidars at TMF and AP both measured O_3 mixing ratios in excess of 100 ppbv within 1 km of the surface, and the in-situ O_3 concentrations at both sites increased to more than 85 ppbv during the night of May 24–25. The AJAX and ozonesonde measurements found up to ~125 ppbv of O_3 between the surface (2 286 m asl) and the minimum range of the TMF lidar. The in-situ measurements at Angel Peak (Langford et al., 2015) also showed coincident decreases in CO and H_2O consistent with descent of UT/LS air to the summit during the night of May 24–25. As is discussed below, some of this O_3 was entrained into the mixed layer the following day and contributed to high surface concentrations in the Las Vegas Valley (~700 m asl) (Langford et al., 2017). In contrast, the surface concentrations in Huntsville remained below 50 ppbv, and the UAH lidar and ozonesonde found no more than ~70 ppbv in the lowest 4 km, despite the apparent deep descent from the UT/LS indicated by HYSPLIT.

6.3. Aircraft measurements

The Alpha Jet took off from Moffett Field at 2023 UT (1 323 Pacific Daylight Time, PDT) on the afternoon of May 24, 2013 and climbed to about 8.5 km asl (FL280) over the San Joaquin Valley (SJV) for the transit flight to TMF. There, it conducted a spiral descent to within 300 m of the surface between 2 112 and 2 132 UT, before returning to MF at an altitude of about 5.2 km asl (FL170). Fig. 8 shows the AJAX measurements as a series of altitude-latitude plots and Fig. 9 displays maps of California and Nevada with the AJAX flight track colorized to reflect the measured O_3, H_2O, CO_2, and CH_4 concentrations. The gaps in Fig. 8b–d were caused by a glitch in the Picarro data acquisition system on the outbound leg. HYSPLIT back trajectories launched from the colored squares in Fig. 8 are also plotted in Figs. 9 and 10.

Fig. 8 shows that AJAX passed through several regions with elevated O_3 during the outbound and inbound flight legs as well as during as the spiral profile over TMF. The origins of this ozone can be inferred from the trajectory analysis and the concomitant behavior of H_2O, CO_2, and CH_4 in the air masses. Upper tropospheric and lower stratospheric air is characterized by very low H_2O, and by low CH_4 (Xiong et al., 2013), which is relatively long-lived and well-mixed in the troposphere, but reacts rapidly with OH in the lower stratosphere (Ehalt et al., 1975).

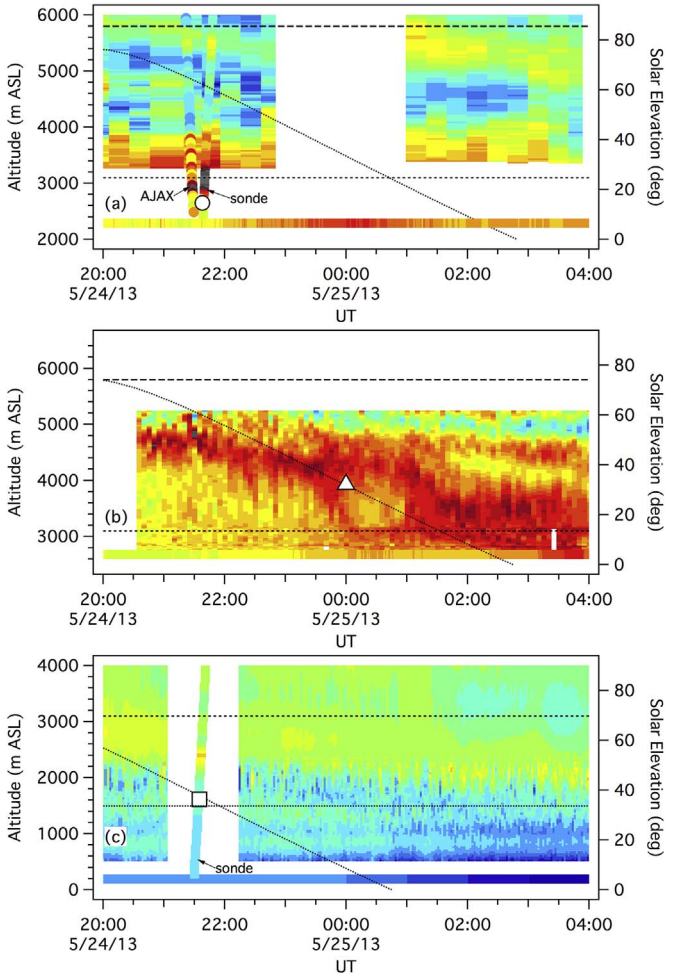

Fig. 6. Same as Fig. 5, but expanded to show the lowest 4 km over the 8-h interval encompassing the afternoon and early evening. The filled symbols show the mixed layer heights determined from the local TOLNet ozonesondes ((a) and (c)), and the KVEF (Las Vegas) sounding (b). The color scale is the same as in Fig. 5. (For interpretation of the references to colour in this figure legend, the reader is referred to the web version of this article.)

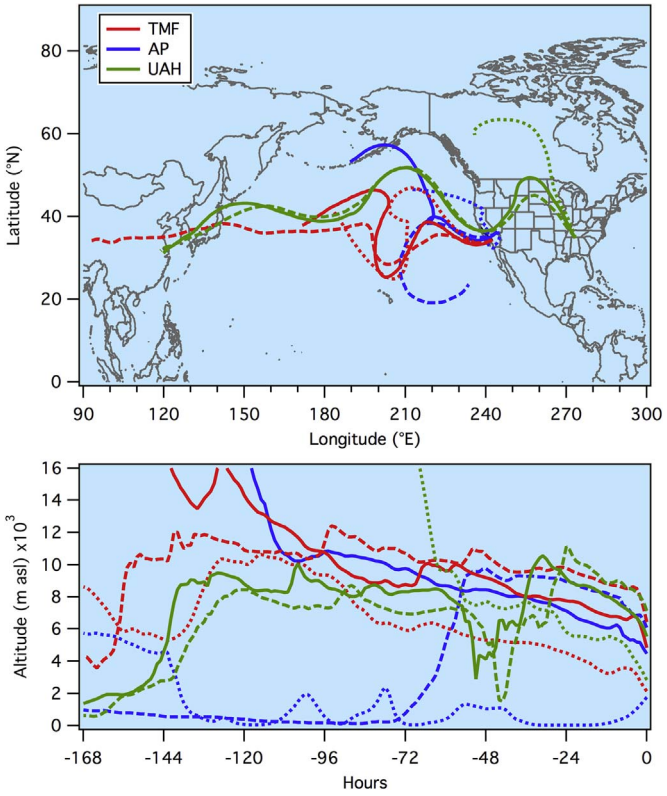

Fig. 7. Complete 7-day HYSPLIT back trajectories (0.5° GDAS meteorology) launched from TMF (red), AP (blue), and UAH (green). The dotted, solid, and dashed lines correspond to launch pressure altitudes of 700, 500, and 400 hPa. (For interpretation of the references to colour in this figure legend, the reader is referred to the web version of this article.)

Low CO_2 can also be diagnostic of UT/LS air since the concentrations are smaller in the lower stratosphere than in the free troposphere during Northern Hemisphere spring (Yates et al., 2013). This attribution is potentially confounded in the lower troposphere, however, since photosynthetic uptake by growing crops or natural vegetation draws down the concentrations of CO_2 near the surface. Conversely, elevated concentrations of CO_2 and CH_4 are usually indicative of surface influences since these compounds are emitted by biomass burning, agricultural activities, and a variety of other anthropogenic processes.

The Alpha Jet passed through a series of narrow layers with very different O_3, CO_2, and CH_4 concentrations between the top of the mixed layer (~1 km asl) and about 5 km asl during the initial ascent from, and the final descent to, Moffett Field. The HYSPLIT back trajectories (green lines in Figs. 9 and 10) suggest that the highest O_3 layers originated from Asia while the interspersed lower O_3 air was recirculated inland from the Pacific Northwest. The aircraft flew through relatively moist air from the Pacific with generally low O_3, CO_2, and CH_4 during most of the outbound flight over the SJV, but entered an expanse of dry air with high CH_4 and CO_2, and slightly elevated O_3 over the Transverse Ranges between the SJV and TMF. The HYSPLIT back trajectories (blue lines) suggest that this air mass was also transported across the Pacific Ocean from Asia. On the return leg, the Alpha Jet passed through another region with high O_3 and CH_4, but depressed CO_2 above the Coast Range at 5.2 km asl. The trajectories from this region (red lines) originated from the stratosphere, but the high CH_4 and low CO_2 suggests there was also co-mingled pollution in this air mass.

Fig. 11 plots profiles of the (a) H_2O, (b) O_3, (c) CO_2, and (d) CH_4 concentrations measured during the AJAX spiral descent over TMF. Fig. 11a also shows the potential temperature and water vapor profiles from the nearly coincident TMF ozonesonde, and Fig. 11b plots the O_3 profiles from AJAX, the ozonesonde, and the TMF lidar. The dashed and dotted red lines in all four plots show the top of the mixed layer inferred from the AJAX and ozonesonde profiles respectively, and the black horizontal dash, long dash, and dot-dash lines show the approximate 700, 500, and 400 hPa levels as in Fig. 3 (TMF lies above the 850 hPa surface). The Alpha Jet passed through a very dry layer with elevated O_3 (purple trajectories in Figs. 9 and 10) between 7.5 and 8 km asl soon after it began its spiral descent. Both CH_4 and CO_2 were slightly depressed in the upper part of this layer compared to the transport layer encountered over the Transverse Ranges, but were enhanced in a narrow altitude range along the lower edge showing the lamination of pollution (or biomass burning) plumes transported from Asia in the upper troposphere and descending stratospheric air. The aircraft and ozonesonde passed through another dry, ozone-rich layer between 5 and 6 km asl, but with no associated enhancement in CH_4 and CO_2. The 500 hPa HYSPLIT back trajectory launched from this region (solid orange line in Fig. 10) suggests that this layer was related to the filament encountered above the Coast Range on the return leg (red line).

The vertical structure in the AJAX profiles became much more complex below 4 km asl. Fig. 11 shows narrow layers of dry, O_3-rich lower stratospheric air with depressed CH_4 and CO_2 alternating with moister lower tropospheric air with higher CH_4 and CO_2 between about 3 and 4 km asl. The aircraft measured peak O_3 mixing ratios in excess of 120 ppbv in a very dry layer with low CH_4 and CO_2 consistent with an UT/LS origin immediately above the top of the mixed layer in good

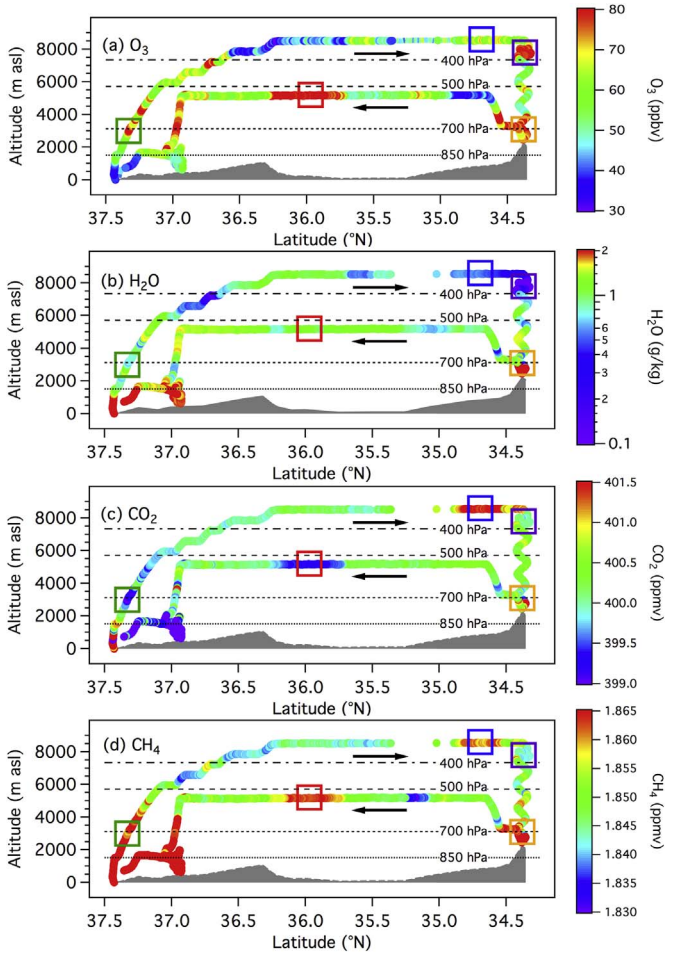

Fig. 8. Latitude-altitude plots colorized according to the Alpha Jet in-situ measurements from the May 24, 2013 flight. (a) O_3, (b) H_2O, (c) CO_2, and (d) CH_4. Note the missing Picarro data between 35.5 and 35.0 °N. The colored boxes mark the origins of the HYSPLIT back trajectories plotted in Fig. 9 and 10. (For interpretation of the references to colour in this figure legend, the reader is referred to the web version of this article.)

agreement with the ozonesonde, but below the minimum range of the lidar. The much lower O_3 and higher H_2O, CO_2, and CH_4 concentrations within the mixed layer provide further evidence that the high O_3 layer near 3 km asl did not originate from the Los Angeles Basin.

Most of the vertical fine structure seen in the AJAX O_3 and H_2O profiles is not seen in the ozonesonde profile. These differences can be explained in part by the roughly 180 m vertical smoothing imparted by the 30-s uncorrected hysteresis of the ECC sensor (Johnson et al., 2002) coupled with the measured 6 m/s ascent rate of the ozonesonde, but most of the fine structure in the AJAX profile is attributed to spatial and temporal variability imparted by gravity waves forced by the synoptic flow over the San Gabriel Mountains (Langford et al., 1996). The resulting small-scale spatial variability is more apparent in the Alpha Jet measurements, which were made over a 10-km diameter spiral, than in the measurements made by the TMF ozonesonde, which was carried to the northeast by the synoptic winds.

6.4. AIRS retrievals

The Atmospheric Infrared Sounder passed over parts of the contiguous U.S. on 6 of the morning descending orbits (0 629–1 124 UT) and 6 of the afternoon ascending orbits (1729–2053 UT) on May 24. Fig. 12 displays the v6 500 hPa (~5.8 km asl) morning and afternoon O_3 mixing ratios retrieved from these orbital swaths. The AIRS retrievals show O_3 mixing ratios in excess of 100 ppbv within each of the two low-pressure centers and the distribution of orange-red colors (> 70 ppbv O_3) shows the same eastward and southward progression of the troughs as the GOES WV retrievals. The AIRS retrievals also show relatively high (> 70 ppbv) O_3 above each of the lidar sites and the AJAX flight track, but resolve none of the horizontal fine structure seen in the aircraft measurements.

The AIRS H_2O, O_3, and CH_4 profiles retrieved from the afternoon overpass of TMF at 20:53 UT are plotted along with the AJAX profiles in Fig. 11. The low-resolution AIRS profiles also miss all of the vertical fine structure seen in the aircraft and lidar measurements. The AIRS O_3 profile in particular bears little resemblance to the aircraft, ozonesonde, and lidar measurements made less than 1 h later, and the agreement is not improved by expanding or shifting the AIRS pixel range used for the comparison. Indeed, the AIRS profile retrieved above AP (not shown), which lies nearly 300 km to the northeast, is almost identical to the TMF profile. The agreement is much better for the relatively unstructured O_3 profile above UAH (Fig. 13), however. The lack of structure in the AIRS profiles is not particularly surprising given that the O_3 retrievals possess less than 1 degree of freedom in the troposphere (He et al., 2011). The Tropospheric Emission Spectrometer (TES) aboard the NASA *Aura* platform provides slightly more degrees of freedom, but TES measurements were unavailable for May 24–25, 2013.

7. Comparison to RAQMS and FLEXPART models

The 12 UT analyses in Figs. 1–4 set the stage for the synoptic observations, but do not directly correspond to the time period of the lidar measurements in Fig. 5. Time-height O_3 distributions directly comparable to the lidar curtain plots in Fig. 5 were calculated from the RAQMS analyses using the reverse domain filling (RDF) technique (Fairlie et al., 2007; Sutton et al., 1994; Yates et al., 2013). RDF calculates 3-dimensional 6-day back trajectories initialized at the model hybrid levels every 5 min using the Langley Trajectory Model (LTM) (Pierce and Fairlie, 1993; Pierce et al., 1994). These back trajectories sample and archive the RAQMS chemical and dynamical quantities with the time averages along a given trajectory mapped back onto the spatial and temporal domains of the TMF, AP, and UAH lidar ozone curtains.

Fig. 14 plots time-height curtain plots of the RAQMS RDF O_3 distributions from the surface to 9 km asl using the same color scale as the lidar measurements in Figs. 5 and 6. The overall structures seen in the lidar plots are reproduced quite well, albeit with much lower resolution. The TMF and AP curtain plots in Fig. 14a and b, respectively, appear very similar to each other, with a layer of high (> 100 ppbv) O_3 descending to ~400 hPa above both sites during the first half of the 24-h observation period. This layer lies well above the maximum range of the TOPAZ lidar (AP), but is consistent with the TMF measurements in Fig. 5a. RAQMS also shows less concentrated (70–80 ppbv) layers descending from the middle troposphere towards the surface of both high elevation sites during the night, with the layer reaching the surface of AP on the morning of May 25 in good agreement with both lidar and in-situ observations. The descending layer remained ~1 km above the surface at TMF, but the model also shows elevated O_3 at the summit.

Like the lidar measurements, the RAQMS RDF distributions for UAH (Fig. 14c) appear qualitatively different from the TMF and AP distributions. The model shows high O_3 above 8 km asl with a less pronounced layer near 6 km as seen in Fig. 5c, and lower O_3 concentrations below 5 km. The RDF concentrations at 700 hPa (dashed line) are smaller than those calculated for 12 UT in Fig. 3b and decrease with time in agreement with the measurements. The model also shows very low O_3 at the surface in good agreement with the in-situ observations.

Time-height curtain plots were also generated by running the FLEXPART model in the backward mode (Seibert and Frank, 2004) from an array of 1 h × 0.5 km time-height cells above each of the lidar location. This technique qualitatively reproduced the influxes to the lower troposphere seen in the TMF and AP lidar observations, but with

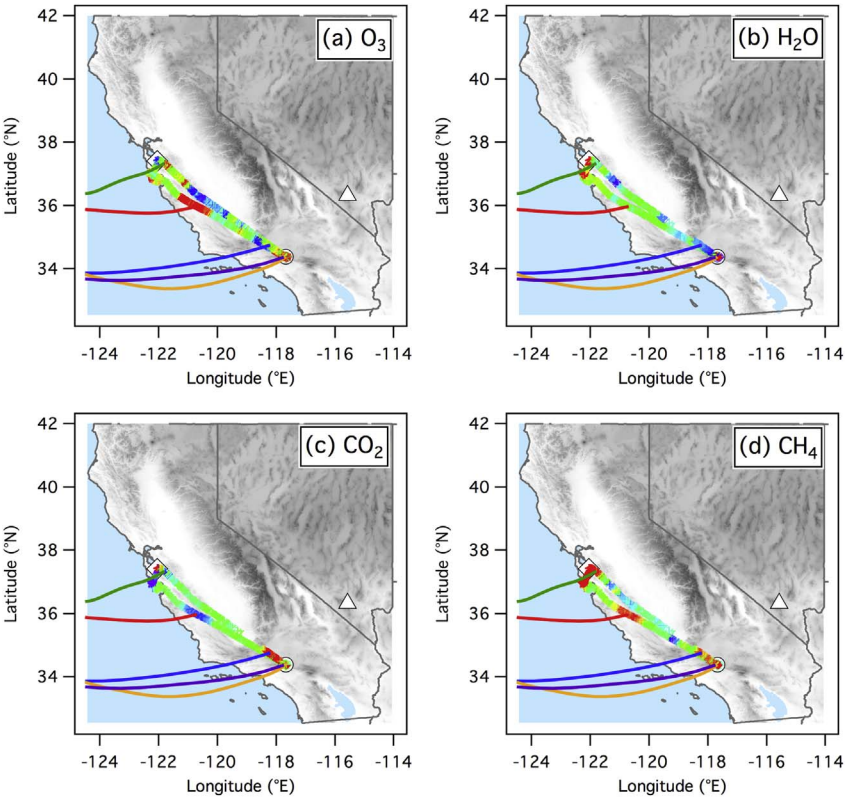

Fig. 9. AJAX flight path colorized by the in-situ O3 measurements. The O3 color scale is the same as in Fig. 5. The colored lines emanating from the flight path show the beginnings of the HYSPLIT back trajectories plotted in Fig. 10. (For interpretation of the references to colour in this figure legend, the reader is referred to the web version of this article.)

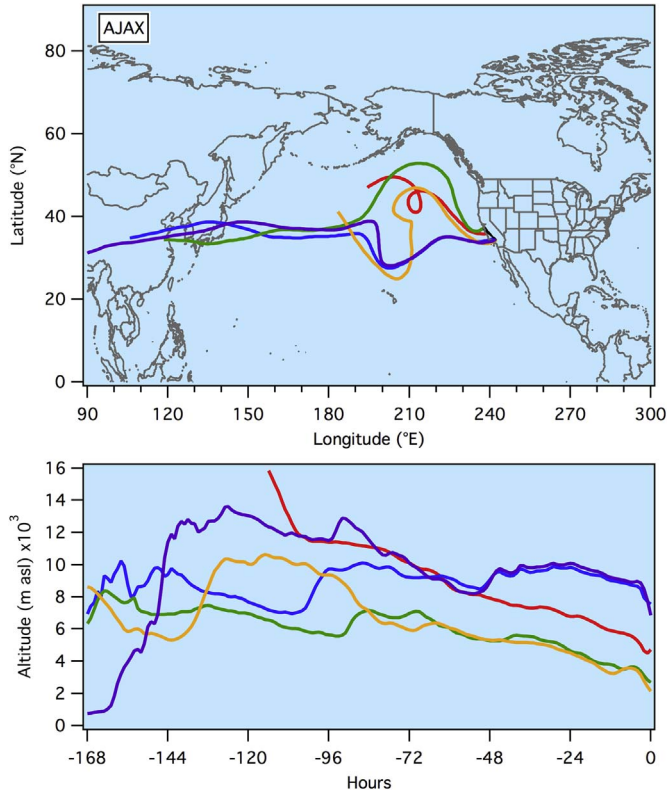

Fig. 10. 7-day HYSPLIT back trajectories launched from the regions of the AJAX flight path indicated in Fig. 8 and 9.

much lower STT O_3 (< 25 ppbv) above TMF and AP than might be expected from the lidar observations. This difference may be an artifact of the higher model resolution of FLEXPART compared to RAQMS; FLEXPART showed much larger STT influxes (> 50 ppbv) within 150 km of both the TMF and AP lidars. In contrast, FLEXPART reproduced the structures seen by the UAH lidar quite well (Fig. 15c) with STT contributions in excess of 30 ppbv in the middle tropospheric layer near 5 km.

8. Comparison to surface air quality monitors

The descent of ozone-rich UT/LS air above the TOLNet lidars in southern California and Nevada during the night of May 24–25, 2013 suggests that the western-most tropopause fold affected a relatively large area. Fig. 16 plots the locations of nearly 1 200 regulatory monitors reporting to the U.S. EPA Air Quality System (AQS) (filled circles) for May 22–27, 2013. The positions of 33 monitors operated by the U.S. National Parks Service (US NPS) are identified by filled triangles. Also plotted are the 8 research monitors belonging to the Nevada Rural Ozone Initiative (NVROI) (Fine et al., 2015; Gustin et al., 2015) (filled squares). Symbols representing monitors that reported MDA8 O_3 concentrations that exceeded the 2008 NAAQS of 75 ppbv in effect at the time of the measurements are colored red while those below the standard are shown in green. Fig. 16 shows that the only monitors exceeding the 75 ppbv NAAQS between May 22 and 27 were located in southern California and Nevada.

The number of regulatory (research) monitors exceeding the 75 ppbv NAAQS increased from 2 (0) on May 23 to 4 (2) on May 24, but then jumped to 10 (3) on May 25 following the descent of the stratospheric intrusion into the lower troposphere. The number of regulatory monitors in exceedance on May 23–26 would have increased to 8, 17, 29, respectively, had the new NAAQS of 70 ppbv been in place.

There were no exceedances on May 22, 26, or 27. Among the regulatory monitors exceeding the standard on May 25 was the California Air Resources Board (CARB) monitor located 40 km to the northeast of TMF in Victorville; the nearest CARB monitor at Hesperia (~15 km) equaled the standard with 75 ppbv. Four of the monitors operated by the Clark County (Nevada) Department of Air Quality in the vicinity of

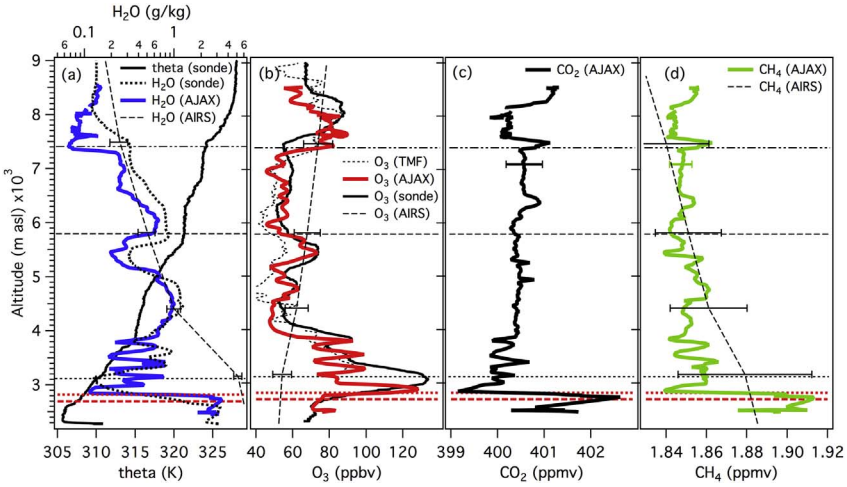

Fig. 11. Ozonesonde, AJAX, and AIRS profiles over TMF on the afternoon of May 24, 2013 profile over TMF. (a) theta and H2O, (b) O3, (c) CO2, and (d) CH4. The black dash, long dash, and dot-dash lines represent the approximate 700, 500, and 400 hPa pressure levels. The red horizontal dashed and dotted lines show the mixed layer height from the ozonesonde and aircraft, respectively. (For interpretation of the references to colour in this figure legend, the reader is referred to the web version of this article.)

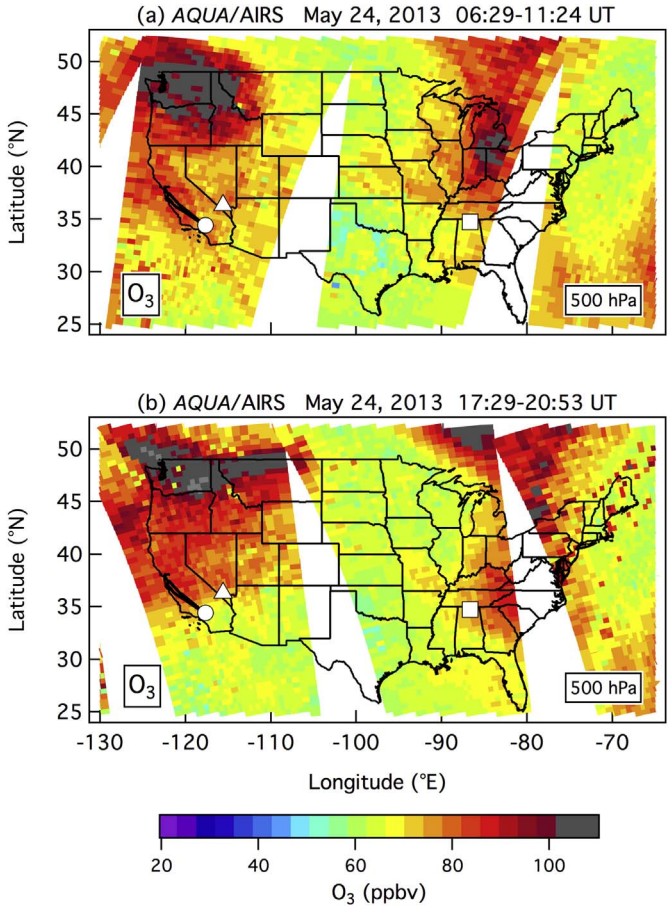

Fig. 12. AIRS version 6, level 2 (non-gridded) 500 hPa O3 concentrations from the May 24, 2013 (a) descending orbits (06:29–11:24 UT) and (b) descending orbits (17:29–20:53 UT). The color scale is the same as in Fig. 5.

AP were also in exceedance of the standard. The MDA8 O_3 measured by the non-regulatory NOAA research monitor on Angel Peak exceeded 75 ppbv on both May 24 and 25, as did 2 and 3, respectively, of the NVROI research monitors.

Although transport of regional pollution from the Los Angeles area almost certainly contributed to the high O_3 levels in the Mojave Desert on May 25, there were no exceedances of the 75 ppbv NAAQS anywhere within the South Coast Air Basin (SoCAB), which includes the Los Angeles Basin, between May 22 and May 27. This is in marked contrast to the pollution export event described by Langford et al. (2010) where MDA8 concentrations well in excess of 100 ppbv were measured within the SoCAB. The measurement of high O_3 concentrations nearly 650 km from Los Angeles at the Great Basin National Park on the Nevada-Utah border strongly suggests that pollution exported from Los Angeles was not the primary source of the high ozone seen in the rural Southwest on May 25.

The spatial distribution of the exceedances is consistent with the descent of O_3-rich UT/LS air seen in the TMF and AP lidar measurements, and by the RAQMS and FLEXPART models. Although several of the exceedances were at high elevation sites, most were at sites below 800 m asl. Indeed, the monitor in Death Valley National Park (125 m asl) reported MDA8 values of 73 and 74 ppbv on May 24 and 25, respectively. These findings are consistent with the hypothesis that there is more potential for entrainment of descending stratospheric air and pollution transported from Asia above the arid southwestern U.S. where the lack of latent heating allows the mixed layers to grow exceptionally deep (Langford et al., 2017).

9. Conclusions

The synoptic snapshot for May 24–25, 2013 presented here illustrates how coordinated ozone lidar vertical profile measurements can help improve our understanding of the processes that influence surface ozone in the U.S. and Canada, particularly when combined with in-situ sampling by a nimble aircraft platform like AJAX. Routine TOLNet ozone lidar measurements can also help state, local, and tribal air quality agencies ascertain the role of background ozone and transport processes during air quality exceedances, and can be used to evaluate tropospheric ozone retrievals from the next generation of satellite-borne sensors like TEMPO. This potential is greatly enhanced when the measurements are guided by models such as RAQMS or FLEXPART operated in routine forecast modes. Coordinated synoptic measurements like those described here can also be used to test the ability of various models (Fiore et al., 2014) to quantify the impacts of stratospheric intrusions and transported pollution on surface ozone, information that is critically needed for the identification of both exceptional and “not-so-exceptional” high ozone events.

The TOLNet lidar measurements described here also show some of the limitations of the lidar systems currently in use for air quality studies. In particular, Figs. 5 and 6 show the importance of coverage in the lowest few hundred meters above the ground to show the relationship of ozone values aloft to the surface measurements. Figs. 5b and 6b show that very low-level measurements are possible if the lidar incorporates a scanner (e.g., the NOAA ESRL TOPAZ lidar), although this method is impractical for most current systems. Another approach would be to combine the lidar operations with in-situ measurements made from

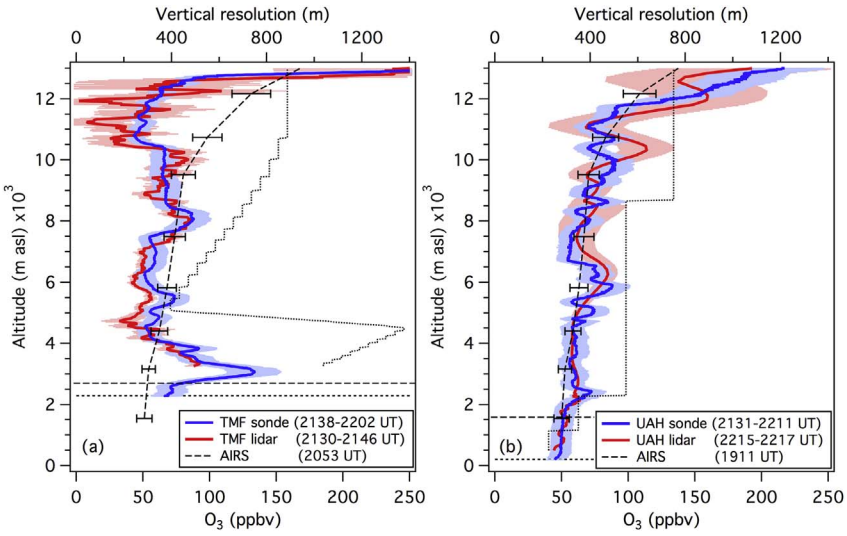

Fig. 13. Ozone profiles measured by the (a) UAH, and (b) TMF lidars (red), and the collocated TOLNet ozonesondes (blue), and the coincident AIRS profiles (black). The UAH and TMF lidar integration times were 2 and 15 min, respectively, and the dotted black lines show the vertical smoothing used in the lidar analyses. The shaded regions show the resulting estimated uncertainties in the lidar (light red) and ozonesonde profiles ± 15% (light blue). The AIRS standard errors are also shown. The ozonesonde time intervals shown in parentheses represent the time required for the balloon to ascend from the surface to 12 km asl. The horizontal short and long dash lines mark the surface elevation and mixed layer heights, respectively. (For interpretation of the references to colour in this figure legend, the reader is referred to the web version of this article.)

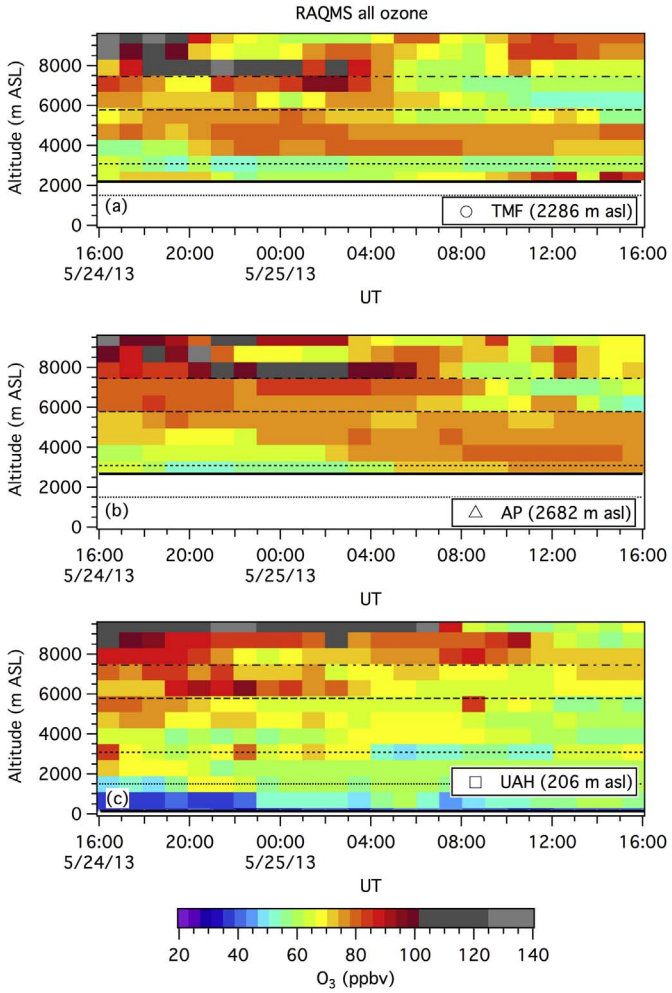

Fig. 14. Time-height curtain plots showing the total O3 distributions above (a) TMF, (b) AP, and (c) UAH calculated from the RAQMS analyses using the reverse domain filling technique. The black dot, dash, long dash, and dot-dash lines represent the approximate 850, 700, 500, and 400 hPa pressure levels. The color scale is the same as in Fig. 5.

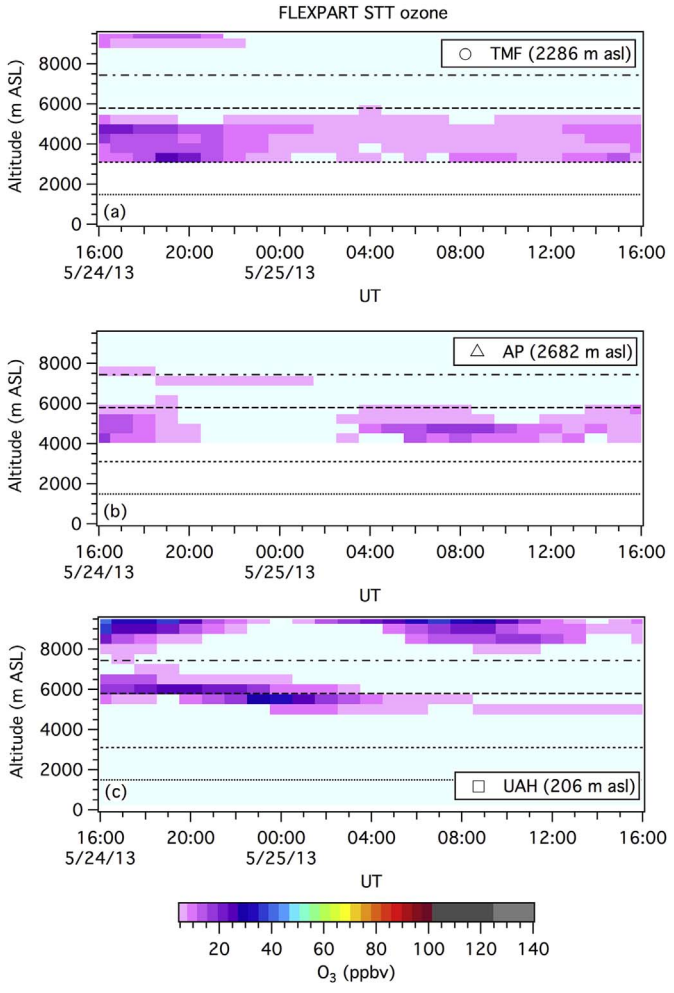

Fig. 15. Time-height curtain plots showing the stratospheric O3 tracer distributions above (a) TMF, (b) AP, and (c) UAH calculated by FLEXPART. The black dot, dash, long dash, and dot-dash lines represent the approximate 850, 700, 500, and 400 hPa pressure levels. The color scale is the same as in Fig. 5.

tethered balloons or unmanned aerial vehicles (UAVs). However, this solution is operator-intensive and is currently limited to daytime measurements. Another serious limitation of most current ozone lidar systems is the need for human operators, which greatly restricts the temporal coverage. This barrier has recently been broken with the development of the Autonomous Mobile Ozone Lidar Instrument for Tropospheric Experiments (AMOLITE) by Environment and Climate Change Canada (ECCC) (Strawbridge et al., 2017), however, and other

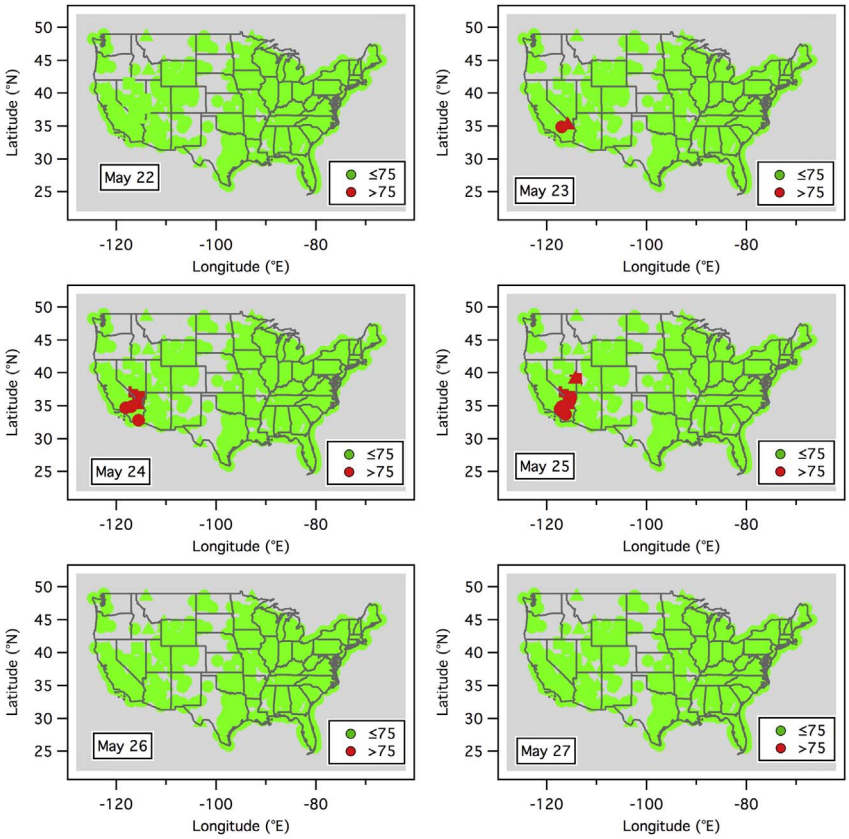

Fig. 16. Map of MDA8 O3 concentrations from the EPA AQS network (filled circles). Regulatory monitors from the U.S. NPS are represented by filled triangles, and research monitors from the NVROI by filled squares (see text). Monitors exceeding the 2008 NAAQS are shown in red. (For interpretation of the references to colour in this figure legend, the reader is referred to the web version of this article.)

autonomous systems may be deployed in the near future.

Acknowledgements

The NOAA/ESRL lidar operations were funded by the NOAA Climate Program Office, Atmospheric Chemistry, Carbon Cycle, and Climate (AC4) Program and the NASA-sponsored Tropospheric Ozone Lidar Network (NNL13AA08I) (TOLNet, http://www-air.larc.nasa.gov/missions/TOLNet/). TOLNet also supported the TMF and UAH lidar efforts. The Las Vegas Ozone Study (LVOS) was funded primarily by the Clark County Department of Air Quality under contract no. CBE 602948-13. The ESRL lidar data from Angel Peak are available at http://www.esrl.noaa.gov/csd/groups/csd3/measurements/lvos/. The authors would like to thank Zheng Li, Mickey Turner, Dennis Randel, and the other staff of the Clark County Department of Air Quality for their assistance and hospitality during LVOS. We also thank Owen Cooper of NOAA/ESRL and CIRES for providing the water vapor imagery, and K. Aikin, S.P. Sandberg, R.M. Marchbanks, and A. Weickmann of NOAA/ESRL and CIRES for technical support. The RAQMS modeling efforts were supported by the NOAA GOES-R Program Office, the NASA Atmospheric Modeling and Analysis Program, and the NASA Applied Science Program. The AJAX project was supported with Ames Research Center Director's funds, and the support and partnership of H211, LLC is gratefully acknowledged. Part of the work described in this paper was carried out at the Jet Propulsion Laboratory, California Institute of Technology, with support for the lidar measurements and ozonesonde launches provided by the NASA Upper Atmosphere Research Program and the NASA Tropospheric Chemistry Program. The authors would like to thank M. Brewer and T. D. Walsh, who assisted in the TMF ozonesonde launches and the collection of the TMF lidar data used here. The authors also gratefully acknowledge the NOAA Air Resources Laboratory (ARL) for the provision of the HYSPLIT transport and dispersion model and/or READY website (http://www.ready.noaa.gov) used in this publication. The views, opinions, and findings contained in this report are those of the author(s) and should not be construed as an official National Oceanic and Atmospheric Administration or U.S. Government position, policy, or decision.

References

Alvarez II, R.J., Senff, C.J., Langford, A.O., Weickmann, A.M., Law, D.C., Machol, J.L., Merritt, D.A., Marchbanks, R.D., Sandberg, S.P., Brewer, W.A., Hardesty, R.M., Banta, R.M., 2011. Development and application of a compact, tunable, solid-state airborne ozone lidar system for boundary layer profiling. J. Atmos. Ocean. Tech. 28, 1258–1272.

Appenzeller, C., Davies, H.C., 1992. Structure of stratospheric intrusions into the troposphere. Nature 358, 570–572.

Attmannspacher, W., Hartmannsgruber, R., 1973. On extremely high values of ozone near the ground. Pure Appl. Geophys 106–108, 1091–1096.

Bian, J.C., Gettelman, A., Chen, H.B., Pan, L.L., 2007. Validation of satellite ozone profile retrievals using Beijing ozonesonde data. J. Geophys. Res. 112.

Bithell, M., Vaughan, G., Gray, L.J., 2000. Persistence of stratospheric ozone layers in the troposphere. Atmos. Environ. 34, 2563–2570.

Bluestein, H.B., 1993. Synoptic-Dynamic Meteorology in Midlatitudes, Volume II Observations and Theory of Weather Systems. Oxford University Press, New York.

Bourqui, M.S., Trepanier, P.Y., 2010. Descent of deep stratospheric intrusions during the IONS August 2006 campaign. J. Geophys. Res. 115.

Brioude, J., Arnold, D., Stohl, A., Cassiani, M., Morton, D., Seibert, P., Angevine, W., Evan, S., Dingwell, A., Fast, J.D., Easter, R.C., Pisso, I., Burkhart, J., Wotawa, G., 2013. The Lagrangian particle dispersion model FLEXPART-WRF version 3.1. Geosci. Model Dev. 6, 1889–1904.

Brioude, J., Cooper, O.R., Trainer, M., Ryerson, T.B., Holloway, J.S., Baynard, T., Peischl, J., Warneke, C., Neuman, J.A., de Gouw, J., Stohl, A., Eckhardt, S., Frost, G.J., McKeen, S.A., Hsie, E.-Y., Fehsenfeld, F.C., Nédélec, P., 2007. Mixing between a stratospheric intrusion and a biomass burning plume. Atmos. Chem. Phys. 7, 4229–4235.

Cho, J.Y.N., Newell, R.E., Bui, T.P., Browell, E.V., Fenn, M.A., Mahoney, M.J., Gregory, G.L., Sachse, G.W., Vay, S.A., Kucsera, T.L., Thompson, A.M., 1999. Observations of convective and dynamical instabilities in tropopuase folds and their contribution to stratsphere-troposphere exchange. J. Geophys. Res. 104, 21549–21568.

Cooper, O.R.C., F Parrish, D.D., Dunlea, E., Hubler, G., Fehsenfeld, F.C., Holloway, J.S., Oltmans, S.J., Johnson, B.J., Wimmers, A., Horowitz, L., 2004. On the life cycle of a stratospheric intrusion and its dispersion into polluted warm conveyor belts. J. Geophys. Res. 109.

Cooper, O.R., Langford, A.O., Parrish, D.D., Fahey, D.W., 2015. Challenges of a lowered US ozone standard. Science 348, 1096–1097.

Cooper, O.R., Oltmans, S.J., Johnson, B.J., Brioude, J., Angevine, W., Trainer, M., Parrish, D.D., Ryerson, T.R., Pollack, I., Cullis, P.D., Ives, M.A., Tarasick, D.W., Al-Saadi, J., Stajner, I., 2011. Measurement of western U.S. baseline ozone from the surface to the tropopause and assessment of downwind impact regions. J. Geophys. Res. 116. http://dx.doi.org/10.1029/2011JD016095.

Danielsen, E.F., 1968. Stratosphere-tropospheric exchange based upon radioactivity, ozone, and potential vorticity. J. Atmos. Sci. 25, 502–518.

Davies, T.D., Schuepbach, E., 1994. Episodes of high ozone concentrations at the Earth's surface resulting from transport down from the upper troposphere/lower stratosphere: a review and case studies. Atmos. Environ. 28, 53–68.

Divakarla, M., Barnet, C., Goldberg, M., Maddy, E., Irion, F., Newchurch, M., Liu, X.P., Wolf, W., Flynn, L., Labow, G., Xiong, X.Z., Wei, J., Zhou, L.H., 2008. Evaluation of Atmospheric Infrared Sounder ozone profiles and total ozone retrievals with matched ozonesonde measurements, ECMWF ozone data, and Ozone Monitoring Instrument retrievals. J. Geophys. Res. 113.

Duncan, B.N., Prados, A.I., Lamsal, L.N., Liu, Y., Streets, D.G., Gupta, P., Hilsenrath, E., Kahn, R.A., Nielsen, J.E., Beyersdorf, A.J., Burton, S.P., Fiore, A.M., Fishman, J., Henze, D.K., Hostetler, C.A., Krotkov, N.A., Lee, P., Lin, M., Pawson, S., Pfister, G., Pickering, K.E., Pierce, R.B., Yoshida, Y., Ziemba, L.D., 2014. Satellite data of atmospheric pollution for U.S. air quality applications: examples of applications, summary of data end-user resources, answers to FAQs, and common mistakes to avoid. Atmos. Environ. 94, 647–662.

Ehalt, D.H., Heidt, L.E., Lueb, R.H., Pollock, W., 1975. Vertical distribution of trace gases in stratosphere. Pure Appl. Geophys. 113, 389–402.

Elbern, H., Hendricks, J., Ebel, A., 1998. A climatology of tropopause folds by global anaylses. Theor. Appl. Clim. 59, 181–200.

Emanuel, K.A., Zivkovic-Rothman, M., 1999. Development and evaluation of a convective scheme for use in climate models. J. Atmos. Sci. 56, 1766–1782.

EPA, 2013. Integrated Science Assessment of Ozone and Related Photochemical Oxidants (Final Report). United States Environmental Protection Agency, Research Triangle Park, NC.

EPA, 2014. Policy Assessment for the Review of the Ozone National Ambient Air Quality Standards. Final Report. United States Environmental Protection Agency, Research Triangle Park, NC.

Fairlie, T.D., Avery, M.A., Pierce, R.B., Al-Saadi, J., Dibb, J., Sachse, G., 2007. Impact of multiscale dynamical processes and mixing on the chemical composition of the upper troposphere and lower stratosphere during the Intercontinental Chemical Transport Experiment-North America. J. Geophys. Res. 112.

Fine, R., Miller, M.B., Burley, J., Jaffe, D.A., Pierce, R.B., Lin, M., Gustin, M.S., 2015. Variability and sources of surface ozone at rural sites in Nevada, USA: results from two years of the Nevada Rural Ozone Initiative. Sci. Total Environ. 530, 471–482.

Fiore, A.M., Oberman, J.T., Lin, M.Y., Zhang, L., Clifton, O.E., Jacob, D.J., Naik, V., Horowitz, L.W., Pinto, J.P., Milly, G.P., 2014. Estimating North American background ozone in U.S. surface air with two independent global models: variability, uncertainties, and recommendations. Atmos. Environ. 96, 284–300.

Fishman, J., Iraci, L.T., Al-Saadi, J., Chance, K., Chavez, F., Chin, M., Coble, P., Davis, C., DiGiacomo, P.M., Edwards, D., Eldering, A., Goes, J., Herman, J., Hu, C., Jacob, D.J., Jordan, C., Kawa, S.R., Key, R., Liu, X., Lohrenz, S., Mannino, A., Natraj, V., Neil, D., Neu, J., Newchurch, M., Pickering, K., Salisbury, J., Sosik, H., Subramaniam, A., Tzortziou, M., Wang, J., Wang, M., 2012. The United States' next generation of atmospheric composition and coastal ecosystem measurements Nasa's geostationary coastal and air pollution events (GEO-CAPE) mission. Bull. Am. Meteorol. Soc. 93, 1547–1566.

Gravelle, C.M., Mecikalski, J.R., Line, W.E., Bedka, K.M., Petersen, R.A., Sieglaff, J.M., Stano, G.T., Goodman, S.J., 2016. Demonstration of a goes-r satellite convective toolkit to "bridge the gap" between severe weather watches and warnings an example from the 20 may 2013 moore, Oklahoma. Tornado Outbreak. Bull. Am. Meteorol. Soc. 97, 69–84.

Gustin, M.S., Fine, R., Miller, M., Jaffe, D., Burley, J., 2015. The Nevada Rural Ozone Initiative (NVROI): insights to understanding air pollution in complex terrain. Sci. Total Environ. 530, 455–470.

Haagenson, P.L., Shapiro, M.A., Middleton, P., Laird, A.R., 1981. A case study relating high ground level ozone to enhanced photochemistry and isentropic transport from the stratosphere. J. Geophys. Res. 86, 5231–5237.

Hamill, P., Iraci, L.T., Yates, E.L., Gore, W., Bui, T.P., Tanaka, T., Loewenstein, M., 2016. A new instrumented airborne platform for atmospheric research. Bull. Am. Meteorol. Soc. 97, 397–404.

Hanna, S.R., 1982. Applications in air pollution modeling. In: Nieuwstadt, F.T.M., van Dop, H. (Eds.), Atmospheric Turbulence and Air Pollution Modelling. D. Reidel Publishing Company, Dordrecht, Holland.

He, H., Tarasick, D.W., Hocking, W.K., Carey-Smith, T.K., Rochon, Y., Zhang, J., Makar, P.A., Osman, M., Brook, J., Moran, M.D., Jones, D.B.A., Mihele, C., Wei, J.C., Osterman, G., Argall, P.S., McConnell, J., Bourqui, M.S., 2011. Transport analysis of ozone enhancement in Southern Ontario during BAQS-Met. Atmos. Chem. Phys. 11, 2569–2583.

Hess, P., Kinnison, D., Tang, Q., 2015. Ensemble simulations of the role of the stratosphere in the attribution of northern extratropical tropospheric ozone variability. Atmos. Chem. Phys. 15, 2341–2365.

Hoskins, B.J., 1982. The mathematical-theory of frontogenesis. Ann. Rev. Fluid Mech. 14, 131–151.

Jaffe, D.A., Wigder, N., Downey, N., Pfister, G., Boynard, A., Reid, S.B., 2013. Impact of wildfires on ozone exceptional events in the western US. Environ. Sci. Technol. 47, 11065–11072.

James, P., Stohl, A., Forster, C., Eckhardt, S., Seibert, P., Frank, A., 2003. A 15-year climatology of stratosphere-troposphere exchange with a Lagrangian particle dispersion model: 2. Mean climate and seasonal variability. J. Geophys. Res. 108. http://dx.doi.org/10.1029/2002JD002639.

Johnson, B.J., Oltmans, S.J., Vömel, H., 2002. Electrochemical concentration cell (ECC) ozonesonde pump efficiency measurements and tests on the sensitivity to ozone of buffered and unbuffered ECC sensor cathode solutions. J. Geophys. Res. 107. http://dx.doi.org/10.1029/2001JD000557.

Johnson, W.B., Viezee, W., 1981. Stratospheric ozone in the lower troposphere-I. presentation and interpretation of aircraft measurements. Atmos. Environ. 15, 1309–1323.

Kaldunski, B., Pierce, R.B., Holloway, T., 2017. When stratospheric ozone hits ground-level regulation: exceptional events in Wyoming bull. Am. Meteorol. Soc. 98, 889–892.

Keyser, D., Shapiro, M.A., 1986. A review of the structure and dynamics of upper-level frontal zones. J. Atmos. Sci. 114, 452–499.

Kirgis, G., Leblanc, T., McDermid, I.S., Walsh, T.D., 2013. Stratospheric ozone interannual variability (1995-2011) as observed by lidar and satellite at mauna loa observatory, HI and table mountain facility, CA. Atmos. Chem. Phys. 13, 5033–5047.

Kuang, S., Burris, J.F., Newchurch, M.J., Johnson, S., Long, S., 2011. Differential absorption lidar to measure subhourly variation of tropospheric ozone profiles. IEEE Trans. Geosci. Rem. Sens. 49, 557–571.

Kuang, S., Newchurch, M.J., Burris, J., Liu, X., 2013. Ground-based lidar for atmospheric boundary layer ozone measurements. Appl. Opt. 52, 3557–3566.

Kuang, S., Newchurch, M.J., Johnson, M.S., Wang, L., Burris, J., Pierce, R.B., Eloranta, E.W., Pollack, I.B., Graus, M., de Gouw, J., Warneke, C., Ryerson, T.B., Markovic, M.Z., Holloway, J.S., Pour-Biazar, A., Huang, G., Liu, X., Feng, N., 2017. Summertime tropospheric ozone enhancement associated with a cold front passage due to stratosphere-to-troposphere transport and biomass burning: simultaneous ground-based lidar and airborne measurements. J. Geophys. Res. 122, 1293–1311.

Kunz, H., Speth, P., 1997. Variability of near-ground ozone concentrations during cold front passages-a possible effect of tropopause folding events. J. Atmos. Chem. 28, 77–95.

Lamb, R.G., 1977. A case study of stratospheric ozone affecting ground-level oxidant concentration. J. Appl. Meteor 16, 780–794.

Langford, A.O., Aikin, K.C., Eubank, C.S., Williams, E.J., 2009. Stratospheric contribution to high surface ozone in Colorado during springtime. Geophys. Res. Lett. 36. http://dx.doi.org/10.1029/2009GL038367.

Langford, A.O., Alvarez, R.J., Brioude, J., Fine, R., Gustin, M.S., Lin, M.Y., Marchbanks, R.D., Pierce, R.B., Sandberg, S.P., Senff, C.J., Weickmann, A.M., Williams, E.J., 2017. Entrainment of stratospheric air and Asian pollution by the convective boundary layer in the southwestern U.S. J. Geophys. Res. 122, 1312–1337.

Langford, A.O., Brioude, J., Cooper, O.R., Senff, C.J., Alvarez, R.J., Hardesty, R.M., Johnson, B.J., Oltmans, S.J., 2012. Stratospheric influence on surface ozone in the Los Angeles area during late spring and early summer of 2010. J. Geophys. Res. 117, D00V06.

Langford, A.O., Proffitt, M.H., VanZandt, T.E., Lamarque, J.-F., 1996. Modulation of tropospheric ozone by a propagating gravity wave. J. Geophys. Res. 101, 26605–26613.

Langford, A.O., Reid, S.J., 1998. Dissipation and mixing of a small-scale stratospheric intrusion in the upper troposphere. J. Geophys. Res. 103, 31265–31276.

Langford, A.O., Senff, C.J., Alvarez, R.J., Banta, R.M., Hardesty, R.M., 2010. Long-range transport of ozone from the Los Angeles Basin: a case study. Geophys. Res. Lett. 37, L06807.

Langford, A.O., Senff, C.J., Alvarez, R.J., Banta, R.M., Hardesty, R.M., Parrish, D.D., Ryerson, T.B., 2011. Comparison between the TOPAZ airborne ozone lidar and in situ measurements during TexAQS 2006. J. Atmos. Ocean. Tech. 28, 1243–1257.

Langford, A.O., Senff, C.J., Alvarez, R.J., Brioude, J., Cooper, O.R., Holloway, J.S., Lin, M.Y., Marchbanks, R.D., Pierce, R.B., Sandberg, S.P., Weickmann, A.M., Williams, E.J., 2015. An overview of the 2013 Las Vegas Ozone Study (LVOS): impact of stratospheric intrusions and long-range transport on surface air quality. Atmos. Environ. 109, 305–322.

Leblanc, T., McDermid, I.S., Walsh, T.D., 2012. Ground-based water vapor raman lidar measurements up to the upper troposphere and lower stratosphere for long-term monitoring. Atmos. Meas. Tech. 5, 17–36.

Lefohn, A.S., Emery, C., Shadwick, D., Wernli, H., Jung, J., Oltmans, S.J., 2014. Estimates of background surface ozone concentrations in the United States based on model-derived source apportionment. Atmos. Environ. 84, 275–288.

Lefohn, A.S., Laurence, J.A., Kohut, R.J., 1988. A comparison of indexes that describe the relationship between exposure to ozone and reduction in the yield of agricultural crops. Atmos. Environ. 22, 1229–1240.

Lefohn, A.S., Wernli, H., Shadwick, D., Limbach, S., Oltmans, S.J., Shapiro, M., 2011. The importance of stratospheric-tropospheric transport in affecting surface ozone concentrations in the western and northern tier of the United States. Atmos. Environ. 45, 4845–4857.

Lefohn, A.S., Wernli, H., Shadwick, D., Oltmans, S.J., Shapiro, M., 2012. Quantifying the importance of stratospheric-tropospheric transport on surface ozone concentrations at high- and low-elevation monitoring sites in the United States. Atmos. Envir 62, 646–656.

Lin, M.Y., Fiore, A.M., Cooper, O.R., Horowitz, L.W., Langford, A.O., Levy, H., Johnson, B.J., Naik, V., Oltmans, S.J., Senff, C.J., 2012. Springtime high surface ozone events over the western United States: quantifying the role of stratospheric intrusions. J. Geophys. Res. 117, D00v22.

Manney, G.L., Stanford, J.L., 1987. On the relation of 6.7 μm water vapour features to isentropic distributions of potential vorticity. Q.J.R. Meteorol. Soc. 113, 1048–1057.

Martin, R.V., 2008. Satellite remote sensing of surface air quality. Atmos. Environ. 42, 21.

McDermid, I.S., Beyerle, G., Haner, D.A., Leblanc, T., 2002. Redesign and improved performance of the tropospheric ozone lidar at the jet propulsion laboratory table mountain facility. Appl. Opt. 41, 7550–7555.

McDermid, I.S., Godin, S.M., Walsh, T.D., 1990. Lidar measurements of stratospheric ozone and intercomparisons and validation. Appl. Opt. 29, 4914–4923.
Mesinger, F., Coauthors, 2006. North American regional Reanalysis. Bull. Amer. Meteor. Soc. 87, 343–360.
Monahan, K.P., Pan, L.L., McDonald, A.J., Bodeker, G.E., Wei, J., George, S.E., Barnet, C.D., Maddy, E., 2007. Validation of AIRS v4 ozone profiles in the UTLS using ozonesondes from Lauder, NZ and Boulder, USA. J. Geophys. Res. 112.
Newchurch, M.J., Ayoub, M.A., Oltmans, S., Johnson, B., Schmidlin, F.J., 2003. Vertical distribution of ozone at four sites in the United States. J. Geophys. Res. 108. http://dx.doi.org/10.1029/2002JD002059.
NOAA, 2014. May 2013 Oklahoma Tornadoes and Flash Flooding, NWS Service Assessment. pp. 62.
Pierce, R.B., Al-Saadi, J.A., Schaack, T., Lenzen, A., Zapotocny, T., Johnson, D., Kittaka, C., Buker, M., Hitchman, M.H., Tripoli, G., Fairlie, T.D., Olson, J.R., Natarajan, M., Crawford, J., Fishman, J., Avery, M., Browell, E.V., Creilson, J., Kondo, Y., Sandholm, S.T., 2003. Regional air quality modeling system (RAQMS) predictions of the tropospheric ozone budget over east Asia. J. Geophys. Res. 108, 8825.
Pierce, R.B., Fairlie, T.D.A., 1993. Chaotic advection in the stratosphere - implications for the dispersal of chemically perturbed air from the polar vortex. J. Geophys. Res. 98, 18589–18595.
Pierce, R.B., Grose, W.L., Russell, J.M., Tuck, A.F., 1994. Evolution of southern-hemisphere spring air masses observed by HALOE. Geophys. Res. Lett. 21, 213–216.
Pierce, R.B., Schaack, T., Al-Saadi, J.A., Fairlie, T.D., Kittaka, C., Lingenfelser, G., Natarajan, M., Olson, J., Soja, A., Zapotocny, T., Lenzen, A., Stobie, J., Johnson, D., Avery, M.A., Sachse, G.W., Thompson, A., Cohen, R., Dibb, J.E., Crawford, J., Rault, D., Martin, R., Szykman, J., Fishman, J., 2007. Chemical data assimilation estimates of continental US ozone and nitrogen budgets during the Intercontinental Chemical Transport Experiment-North America. J. Geophys. Res. 112.
Pittman, J.V., Pan, L.L., Wei, J.C., Irion, F.W., Liu, X., Maddy, E.S., Barnet, C.D., Chance, K., Gao, R.S., 2009. Evaluation of AIRS, IASI, and OMI ozone profile retrievals in the extratropical tropopause region using in situ aircraft measurements. J. Geophys. Res. 114.
Proffitt, M.H., Langford, A.O., 1997. Ground-based differential absorption lidar system for day or night measurements of ozone throughout the free troposphere. Appl. Opt. 36, 2568–2585.
Reed, R.J., Danielsen, E.F., 1959. Fronts in the vicinity of the tropopause. Arch. Meteorol. Geophys. Bioklim. 11, 1–17.
Rolph, G., Stein, A., Stunder, B., 2017. Real-time environmental applications and display sYstem: ready. Environ. Model. & Softw. 95, 210–228.
Ryoo, J.M., Johnson, M.S., Iraci, L.T., Yates, E.L., Gore, W., 2017. Investigating sources of ozone over California using AJAX airborne measurements and models.: assessing the contribution from longrange transport. Atmos. Environ. 155, 53–67.
Schaack, T.K., Zapotocny, T.H., Lenzen, A.J., Johnson, D.R., 2004. Global climate simulation with the university of Wisconsin global hybrid isentropic coordinate model. J. Clim. 17, 2998–3016.
Seibert, P., Frank, A., 2004. Source-receptor matrix calculation with a Lagrangian particle dispersion model in backward mode. Atmos. Chem. Phys. 4, 13.
Shapiro, M.A., 1980. Turbulent mixing within tropopause folds as a mechanism for the exchange of constituents between the stratosphere and troposphere. J. Atmos. Sci. 37, 994–1004.
Skerlak, B., Sprenger, M., Wernli, H., 2014. A global climatology of stratosphere-troposphere exchange using the ERA-Interim data set from 1979 to 2011. Atmos. Chem. Phys. 14, 913–937.
State of Wyoming, 2013. Exceptional Event Demonstration Package for the Environmental Protection Agency: Big Piney and Boulder, Wyoming Ozone Standard Exceedances June 14, 2012. Department of Environmental Quality/Air Quality Division.
Stein, A.F., Draxler, R.R., Rolph, G.D., Stunder, B.J.B., Cohen, M.D., Ngan, F., 2015. NOAA'S HYSPLIT Atmospheric transport and dispersion modeling system. Bull. Amer. Meteor. Soc. 96, 2059–2077.
Stohl, A., Forster, C., Frank, A., Seibert, P., Wotawa, G., 2005. Technical note: the Lagrangian particle dispersion model FLEXPART version 6.2. Atmos. Chem. Phys. 5, 2461–2474.
Stohl, A., Spichtinger-Rakowsky, N., Bonasoni, P., Feldmann, H., Memmesheimer, M., Scheel, H.E., Trickl, T., Hubener, S., Ringer, W., Mandl, M., 2000. The influence of stratospheric intrusions on alpine ozone concentrations. Atmos. Environ. 34, 1323–1354.
Strawbridge, K.B., Firanski, B.J., Travis, M.S., 2017. Autonomous Ozone, Aerosol, and Water Vapor Profiling of the Atmosphere. SPIE Newsroom.
Sullivan, J.T., McGee, T.J., DeYoung, R., Twigg, L.W., Sumnicht, G.K., Pliutau, D., Knepp, T., Carrion, W., 2015a. Results from the NASA GSFC and LaRC ozone lidar intercomparison: new mobile tools for atmospheric research. J. Atmos. Ocean. Tech. 32, 1779–1795.
Sullivan, J.T., McGee, T.J., Leblanc, T., Sumnicht, G.K., Twigg, L.W., 2015b. Optimization of the GSFC TROPOZ DIAL retrieval using synthetic lidar returns and ozonesondes - Part 1: algorithm validation. Atmos. Meas. Tech. 8, 4133–4143.
Sutton, R.T., Maclean, H., Swinbank, R., O'Neill, A., Taylor, F.W., 1994. High-resolution stratospheric tracer fields estimated from satellite-observations using Lagrangian trajectory calculations. J. Atmos. Sci. 51, 2995–3005.
Tanaka, T., Yates, E., Iraci, L.T., Johnson, M.S., Gore, W., Tadic, J., Loewenstein, M., Kuze, A., Frankenberg, C., Butz, A., Yoshida, Y., 2016. Two-year comparison of airborne measurements of CO2 and CH4 with GOSAT at railroad valley, Nevada. Geoscience and remote sensing. IEEE Trans. 54, 4367–4375.
Trickl, T., Vogelmann, H., Giehl, H., Scheel, H.E., Sprenger, M., Stohl, A., 2014. How stratospheric are deep stratospheric intrusions? Atmos. Chem. Phys. 14, 9941–9961.
U.S. Environmental Protection Agency, 2007. Treatment of data influenced by exceptional events. In: Federal Register. Environmental Protection Agency, U.S., pp. 13560–13581.
U.S. Environmental Protection Agency, 2015. In: National Ambient Air Quality Standards for Ozone: Final Rule. Environmental Protection Agency, U.S. EPA–HQ–OAR–2008–0699; FRL–9933–18– OAR, Federal Register.
U.S. Environmental Protection Agency, 2016. In: Treatment of Data Influenced by Exceptional Events. Environmental Protection Agency, U.S., pp. 68216–68282 Federal Register.
Viezee, W., Johnson, W.B., Singh, H.B., 1983. Stratospheric ozone in the lower troposphere-II. assessment of downward flux and ground-level impact. Atmos. Environ. 17, 1979–1993.
Warneke, C., Trainer, M., de Gouw, J.A., Parrish, D.D., Fahey, D.W., Ravishankara, A.R., Middlebrook, A.M., Brock, C.A., Roberts, J.M., Brown, S.S., Neuman, J.A., Lerner, B.M., Lack, D., Law, D., Hubler, G., Pollack, I., Sjostedt, S., Ryerson, T.B., Gilman, J.B., Liao, J., Holloway, J., Peischl, J., Nowak, J.B., Aikin, K.C., Min, K.E., Washenfelder, R.A., Graus, M.G., Richardson, M., Markovic, M.Z., Wagner, N.L., Welti, A., Veres, P.R., Edwards, P., Schwarz, J.P., Gordon, T., Dube, W.P., McKeen, S.A., Brioude, J., Ahmadov, R., Bougiatioti, A., Lin, J.J., Nenes, A., Wolfe, G.M., Hanisco, T.F., Lee, B.H., Lopez-Hilfiker, F.D., Thornton, J.A., Keutsch, F.N., Kaiser, J., Mao, J.Q., Hatch, C.D., 2016. Instrumentation and measurement strategy for the NOAA SENEX aircraft campaign as part of the Southeast Atmosphere Study 2013. Atmos. Meas. Tech. 9, 3063–3093.
Wei, J.C., Pan, L.L., Maddy, E., Pittman, J.V., Divarkarla, M., Xiong, X.Z., Barnet, C., 2010. Ozone profile retrieval from an advanced infrared sounder: experiments with tropopause-based climatology and optimal estimation approach. J. Atmos. Ocean. Tech. 27, 1123–1139.
Wernli, H., Bourqui, M., 2002. A Lagrangian "1-year climatology' of (deep) cross-tropopause exchange in the extratropical Northern Hemisphere. J. Geophys. Res. 107.
Wernli, H., Davies, H.C., 1997. A Lagrangian-based analysis of extratropical cyclones. I: the method and some applications. Q. J. R. Meteorol. Soc. 123, 467–489.
Xiong, X.Z., Barnet, C., Maddy, E., Wofsy, S.C., Chen, L.F., Karion, A., Sweeney, C., 2013. Detection of methane depletion associated with stratospheric intrusion by atmospheric infrared sounder (AIRS). Geophys. Res. Lett. 40, 2455–2459.
Yates, E.L., Iraci, L.T., Austerberry, D., Pierce, R.B., Roby, M.C., Tadic, J.M., Loewenstein, M., Gore, W., 2015. Characterizing the impacts of vertical transport and photochemical ozone production on an exceedance area. Atmos. Environ. 109, 342–350.
Yates, E.L., Iraci, L.T., Roby, M.C., Pierce, R.B., Johnson, M.S., Reddy, P.J., Tadic, J.M., Loewenstein, M., Gore, W., 2013. Airborne observations and modeling of springtime stratosphere-to-troposphere transport over California. Atmos. Chem. Phys. 13, 12481–12494.
Yates, E.L., Schiro, K., Lowenstein, M., Sheffner, E.J., Iraci, L.T., Tadić, J.M., Kuze, A., 2011. Carbon dioxide and methane at a Desert site—a case study at railroad valley playa, Nevada, USA. Atmosphere 2, 702.
Zhang, L., Jacob, D.J., Downey, N.V., Wood, D.A., Blewitt, D., Carouge, C.C., van Donkelaar, A., Jones, D.B.A., Murray, L.T., Wang, Y.X., 2011. Improved estimate of the policy-relevant background ozone in the United States using the GEOS-Chem global model with 1/2 degrees x 2/3 degrees horizontal resolution over North America. Atmos. Environ. 45, 6769–6776.
Zhang, L., Jacob, D.J., Yue, X., Downey, N.V., Wood, D.A., Blewitt, D., 2014. Sources contributing to background surface ozone in the US Intermountain West. Atmos. Chem. Phys. 14, 5295–5309.
Zoogman, P., Jacob, D.J., Chance, K., Liu, X., Lin, M., Fiore, A., Travis, K., 2014. Monitoring high-ozone events in the US Intermountain West using TEMPO geostationary satellite observations. Atmos. Chem. Phys. 14, 6261–6271.
Zoogman, P., Jacob, D.J., Chance, K., Zhang, L., Le Sager, P., Fiore, A.M., Eldering, A., Liu, X., Natraj, V., Kulawik, S.S., 2011. Ozone air quality measurement requirements for a geostationary satellite mission. Atmos. Environ. 45, 7143–7150.